Fault and Stress Analysis: User's manual for the Fsa software

Bernard Célérier

Version 1.0

2025-07-27

Contents

List of Tables

List of Figures

Part I

Introduction & conventions

Chapter 1

General Conventions

1.1 Introduction

This chapter lays out general definitions and conventions that are useful for the following chapters and that were introduced in previous work (*Célérier*, 1988; *Tajima and Célérier*, 1989; *Célérier*, 1995; *Célérier and Séranne*, 2001; *Burg et al.*, 2005; *Célérier*, 2010).

1.2 Notations

We use a super script convention where the matrix representing a frame or operator F in the reference frame H is written $\mathbf{F^H}$. In the case F is a frame, $F = (\vec{f}_1, \vec{f}_2, \vec{f}_3)$, the j^{th} column of $\mathbf{F^H}$ is made of the coordinates of $\vec{f}_j$ in the H frame.

1.3 Parameters

A list of parameters used throughout this manual is given in Table 1.1. More parameters with limited scope are further defined within chapters.

1.4 Geographical G frame

A right handed geographical frame, G, is built with the unit vectors $\vec{g}_1, \vec{g}_2, \vec{g}_3$ pointing north, east and down respectively: $G = (\vec{g}_1, \vec{g}_2, \vec{g}_3)$ (*Tajima and Célérier*, 1989; *Célérier*, 2008, 2010).

Table 1.1: Parameters used in this document

Symbol	Comments
	Geographical frame
$G = (\vec{g_1}, \vec{g_2}, \vec{g_3})$	Geographical right-handed frame: $\vec{g_1}, \vec{g_2}, \vec{g_3}$ are unit vectors pointing north, east and down, respectively.
	Fault and slip data
$N = (\vec{n_1}, \vec{n_2}, \vec{n_3})$	Fault plane frame: $\vec{n_1}, \vec{n_2}, \vec{n_3}$ are unit vectors. $\vec{n_1}, \vec{n_2}$ are within the plane and pointing along the strike and dip directions, and $\vec{n_3}$ is the downward pointing normal to the plane.
$E = (\vec{e_1}, \vec{e_2}, \vec{e_3})$	Fault plane and slip frame: $\vec{e_1}, \vec{e_2}, \vec{e_3}$ are unit vectors. $\vec{e_1}, \vec{e_2}$ are within the plane; $\vec{e_1}$ is along the slip direction and $\vec{e_3}$ is the downward pointing normal to the plane.
α	Strike
δ	Dip
λ	Rake
	Stress tensor
$\sigma_1 \geqslant \sigma_2 \geqslant \sigma_3$	Principal stress magnitudes (positive compression)
$S = (\vec{s_1}, \vec{s_2}, \vec{s_3})$	Principal stress directions (right-handed frame)
$\widehat{\mathbf{\Sigma}}$	Full stress tensor
$\widehat{\mathbf{\Sigma}}_\mathbf{r}$	Reduced stress tensor
$\widehat{\mathbf{I}}$	Identity tensor
$\mathbf{\Sigma^S}$	Matrix of $\widehat{\mathbf{\Sigma}}$ in S
$\mathbf{\Sigma_r^S}$	Matrix of $\widehat{\mathbf{\Sigma}}_\mathbf{r}$ in S
$\mathbf{S^G}$	Change of basis matrix from G to S: j$^{\text{th}}$ column is made of the coordinates of $\vec{s_j}$ in frame G
θ, φ, ψ	Euler's angles used to define $\mathbf{S^G}$
$r_0 = \dfrac{\sigma_1 - \sigma_2}{\sigma_1 - \sigma_3}$	Stress tensor aspect ratio
$s_0 = \dfrac{\sigma_1 - \sigma_3}{\sigma_1}$	Normalized stress difference
	Friction
ϕ_0	Friction angle
μ	Coefficient of friction $\quad \mu = \tan(\phi_0)$

Part II

Data

Chapter 2

Fault and slip data

2.1 Introduction

This chapter

1. introduces two reference frames used to define fault and slip data orientation,
2. discusses four ways of recording the orientation of fault and slip data that can be handled by FSA, and
3. lays out the eight different types of fault and slip data that are handled by FSA.

2.2 Fault and slip frames

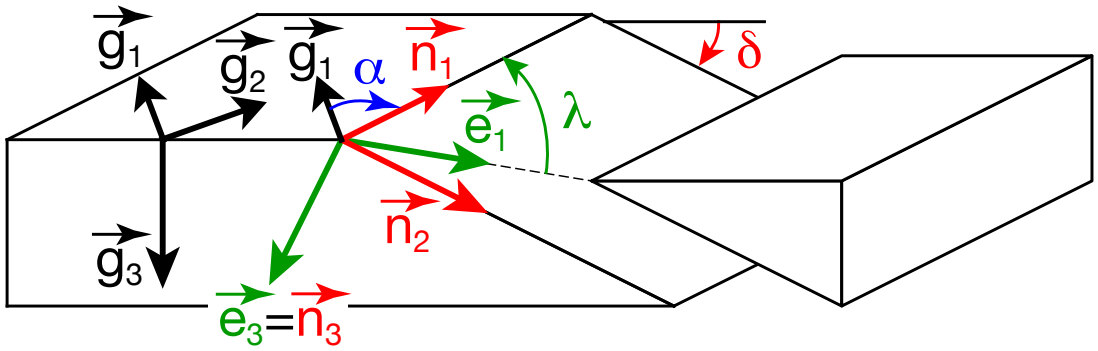

Figure 2.1: Fault and slip orientation: strike, α, dip δ, and rake λ. Geographical frame $G = (\vec{g_1}, \vec{g_2}, \vec{g_3})$, fault plane frame $N = (\vec{n_1}, \vec{n_2}, \vec{n_3})$, and fault and slip frame $E = (\vec{e_1}, \vec{e_2}, \vec{e_3})$.

To define fault and slip orientation, it is convenient to introduce two orthogonal frames of unit vectors, N and E (Fig. 2.1).

2.2.1 Fault plane N frame

The first orthogonal frame of unit vectors, $N = (\vec{n_1}, \vec{n_2}, \vec{n_3})$, is attached to the fault plane only (*Tajima and Célérier*, 1989; *Célérier*, 1995; *Célérier and Séranne*, 2001; *Célérier*, 2010):

- $\vec{n_1}$ is along the strike direction and so that the plane dips to its right,
- $\vec{n_2}$ is within the plane and along the dip direction, and
- $\vec{n_3}$ is the downward pointing normal to the plane, so that N is right-handed.

2.2.2 Fault and slip E frame

The second orthogonal frame of unit vectors, $E = (\vec{e_1}, \vec{e_2}, \vec{e_3})$, is attached to the fault plane and its associated slip direction (*McKenzie*, 1969; *Célérier*, 1988; *Tajima and Célérier*, 1989; *Célérier*, 2010; *Célérier et al.*, 2012):

- $\vec{e_1}$ is along the slip direction of the hanging wall with respect to the footwall,
- $\vec{e_3}$ is the downward pointing normal to the plane, and
- $\vec{e_2}$ is normal to both $\vec{e_1}$ and $\vec{e_3}$ and chosen so that E is right-handed

2.3 Recording fault and slip orientation

Fsa can handle four manners of recording slip data orientations that are detailed below. The first one is mainly used for fault plane solutions, whereas the three other ones are mainly used for outcrop field measurements.

2.3.1 Strike, dip, rake with Aki & Richards' convention

This representation is extensively used in seismological databases and corresponds to the internal representation within Fsa. It is concise, fully numerical, unambiguous, and clearly and precisely defined in *Aki and Richards* (1980) p.106 or *Aki and Richards* (2002) p. 101. Three angles are recorded (Fig. 2.1):

- strike, α, is in [0,360] and is the azimuth of the horizontal direction chosen so that the plane dips to the right, i.e. $\vec{n_1}$,
- dip, δ, is the plunge of $\vec{n_2}$ in [0,90], and
- defining the slip direction as that of the hanging wall with respect to the footwall, rake, λ, is the angle between the strike, $\vec{n_1}$, and the slip direction, $\vec{e_1}$, measured contra-clockwise from above.

Example: 30 60 -20

The three angles, α, δ, and $-\lambda$ are equivalent to *Euler*'s (1767) angles (Fig. 2.2) :

- a first rotation of angle α around $\vec{g_3}$ transforms the geographical frame, G, into the frame $U = (\vec{u_1}, \vec{u_2}, \vec{u_3})$,
- a second rotation of angle δ around $\vec{u_1}$ transforms U into N, and
- a third rotation of angle $-\lambda$ around $\vec{n_3}$ transforms N into E.

The relationship between rake, λ, taken in [-180,180] and fault movement type is given in Table 2.1 .

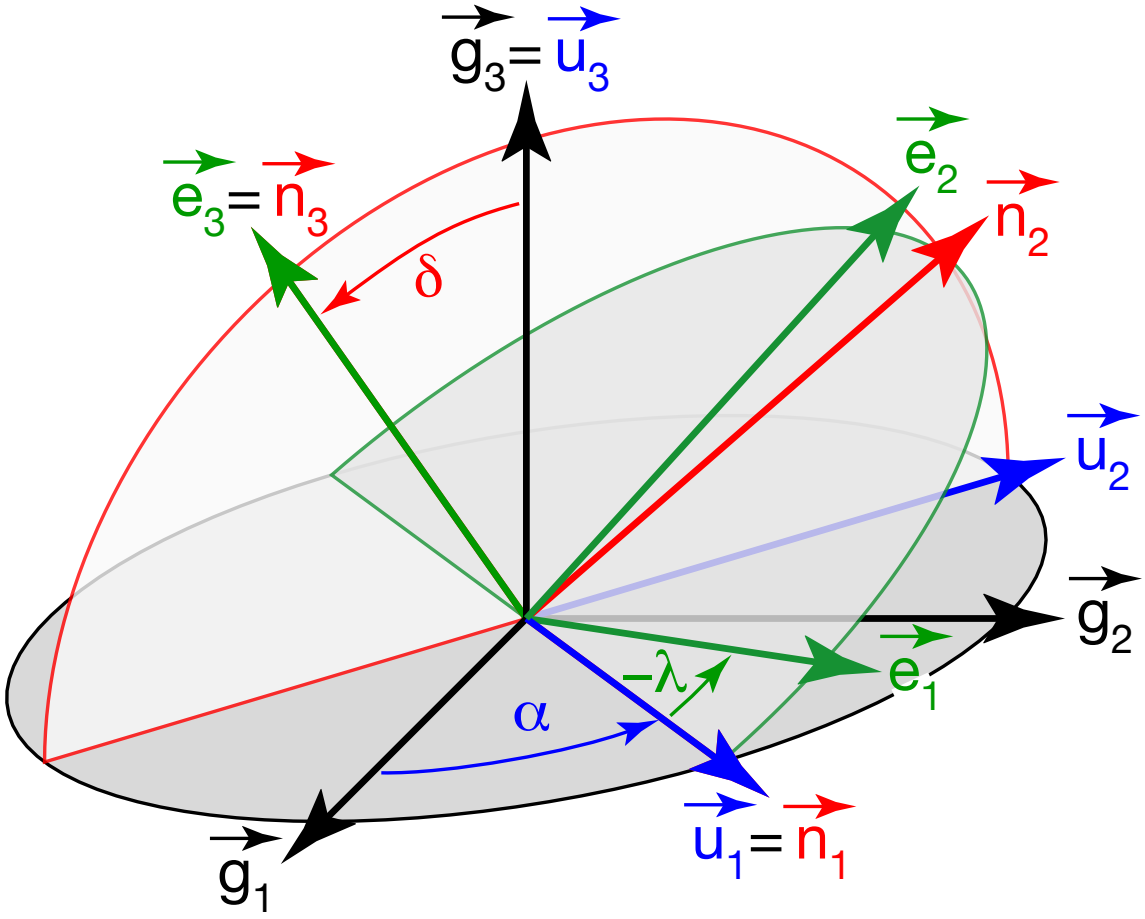

Figure 2.2: *Euler*'s (1767) angles transforming the geographical frame $G = (\vec{g_1}, \vec{g_2}, \vec{g_3})$ into the fault and slip frame $E = (\vec{e_1}, \vec{e_2}, \vec{e_3})$ through 3 successive rotations of angles α, δ, and $-\lambda$. The intermediate stages are $U = (\vec{u_1}, \vec{u_2}, \vec{u_3})$ and $N = (\vec{n_1}, \vec{n_2}, \vec{n_3})$.

Table 2.1: Rake intervals versus fault movement types

	Sinistral	Dextral
Reverse	[0 , 90]	[90, 180]
Normal	[-90, 0]	[-180, -90]

2.3.2 Field measurements: strike, dip, pitch

This is one of two representations used for recording field structural measurements in the former Structural Geology Lab of Montpellier and implemented in the original FAILLE program (*Etchecopar et al.*, 1981; *Etchecopar*, 1984). It is appropriate for high dip planes where pitch measurements are accurate, but must be replaced by the strike, dip, trend representation for low dip planes where pitch measurements become inaccurate. Contrary to many other formats, it does not require any correction on strike angle measurements, but take them as directly read on the compass. This eliminates many sources of error, but requires to record two quadrants orientations. Six parameters, 3 numbers and 3 words, are recorded:

- Strike is in [0,360] and is one of the two possible azimuths of the horizontal direction
- Dip angle is in [0,90]
- Dip direction is indicated by a quadrant: North, South, East or West
- Pitch is the angle in [0,90] between one of the strike direction and the slip direction; this strike direction is chosen among the two opposite possibilities so that the pitch angle remains acute.
- Pitch quadrant indicates the quadrant where lies the strike direction chosen to measure pitch. It is recorded as North, South, East or West
- Movement type: Normal, Reverse, Dextral, Sinistral

Example (same as previous example):
30 60 East, pitch 20 North, Sinistral

2.3.3 Field measurements: strike, dip, trend

This is the other of two representations used for recording field structural measurements in the former Structural Geology Lab of Montpellier and implemented in the original FAILLE program (*Etchecopar et al.*, 1981; *Etchecopar*, 1984). It is appropriate for low dip planes where trend measurements are accurate, but must be replaced by the strike, dip, pitch representation for high dip planes where trend measurements become inaccurate. It does not require any correction on strike angle measurements, but take them as directly read on the compass. This eliminates many sources of error, but requires to record one quadrant orientation. Five parameters, 3 numbers and 2 words, are recorded:

- Strike is in [0,360] and is one of the two possible azimuths of the horizontal direction.

- Dip angle is in [0,90]
- Dip direction is indicated by a quadrant: North, South, East or West
- Trend is one of the two azimuths in [0,360] of the vertical plane that contains the slip direction.
- Movement type: Normal, Reverse, Dextral, Sinistral

Example (same as previous examples):
30 60 East, trend 40, Sinistral

2.3.4 Field measurements: dip direction, dip, trend, plunge

This representation is more convenient with certain types of compass that directly indicate dip direction or can measure plunge more easily than pitch. Five parameters, 4 numbers and 1 word, are recorded:

- Dip direction is in [0,360].
- Dip angle is in [0,90]
- Slip direction trend in [0,360]
- Slip direction plunge in [0,90]
- Movement type: Normal, Reverse, Dextral, Sinistral

Example (same as previous examples):
120 60, 40 17, Sinistral

2.4 Fault slip data types

Data type defines the amount of information contained in the data and constrains the operations that the software will be allowed to do with these data. FSA can handle 8 data types that are listed in Table 2.2. Each data type is tagged in the software with an identification integer (ID) which given in the right column of Table 2.2.

2.4.1 Plane

Definition: Plane orientation only. Can be used for fractures, faults without slip indicator, veins, foliations or beddings.

2.4.2 Plane and 1 space coordinate

Definition: Plane orientation with one associated space coordinate. This is useful for fracture or bedding measurements along a linear outcrop, such as a roadcut, or from a borehole.

Table 2.2: Fault slip data types

Data types	ID
Fault and slip	100
Fault and slip with rake range	110
Fault and slip with bedding	150
Original and restored fault and slip with bedding	200
Fault plane solution	300
Fault plane solution and 3 coordinates	313
Plane	400
Plane and 1 coordinate	411

2.4.3 Fault and slip

Definition: Fault plane and slickenline orientation. This is the default type when starting Fsa.

2.4.4 Fault and slip with rake range

Definition: Fault plane with slip known within a rake range only.

2.4.5 Fault and slip with bedding

Definition: Fault plane, slickenline and associated bedding orientations. This combination of data allows to restore the structures to the situation where bedding is horizontal.

2.4.6 Original and restored fault and slip with bedding

Definition: Original fault plane, slickenline and associated bedding orientations together with fault plane and slickenline orientations restored for horizontal bedding. This is an output type that is obtained after Fsa has restored orientations of with fault and slip with bedding type.

2.4.7 Fault plane solution

Definition: Earthquake fault plane solution. Given either as one nodal plane or as both nodal planes.

2.4.8 Fault plane solution and 3 space coordinates

Definition: Earthquake fault plane solution with full hypocenter location. The location may be given in Cartesian (x, y, z) or geographical (longitude, latitude, depth) coordinates.

Chapter 3

Stress data

3.1 Introduction

This chapter

1. introduces the principal stress directions frame,
2. discusses the stress tensor parameters, and
3. lays out the six different types of stress data that are handled by FSA.

3.2 Principal stress directions S frame

We define three unit vectors, $\vec{s_1}$, $\vec{s_2}$, and $\vec{s_3}$, along the eigenvectors of the stress tensor, $\widehat{\boldsymbol{\Sigma}}$, i.e., along the principal stress directions,

- so that they correspond to the eigenvalues, i.e., the principal stress magnitudes, ordered as $\sigma_1 \geqslant \sigma_2 \geqslant \sigma_3$, with the rock mechanics convention that compression is positive, and
- so that the frame $S = (\vec{s_1}, \vec{s_2}, \vec{s_3})$ is right-handed.

3.3 Stress tensor representations

The full stress tensor, $\widehat{\boldsymbol{\Sigma}}$, can be decomposed as:

$$\widehat{\boldsymbol{\Sigma}} = (\sigma_1 - \sigma_3) \cdot \widehat{\boldsymbol{\Sigma}}_{\mathbf{r}} + \sigma_3 \cdot \widehat{\mathbf{I}} \tag{3.1}$$

where $\widehat{\boldsymbol{\Sigma}}_{\mathbf{r}}$ is the reduced stress tensor and $\widehat{\mathbf{I}}$ the identity tensor. $\widehat{\boldsymbol{\Sigma}}$ and $\widehat{\boldsymbol{\Sigma}}_{\mathbf{r}}$ share the same eigenvectors, $\vec{s_1}$, $\vec{s_2}$, and $\vec{s_3}$, but have different eigenvalues: in the S frame, the full stress

tensor, $\widehat{\boldsymbol{\Sigma}}$, is represented by the matrix $\boldsymbol{\Sigma}^{\mathbf{S}}$

$$\boldsymbol{\Sigma}^{\mathbf{S}} = \begin{bmatrix} \sigma_1 & 0 & 0 \\ 0 & \sigma_2 & 0 \\ 0 & 0 & \sigma_3 \end{bmatrix} \tag{3.2}$$

whereas the reduced stress tensor, $\widehat{\boldsymbol{\Sigma}}_{\mathbf{r}}$, is represented by $\boldsymbol{\Sigma}^{\mathbf{S}}_{\mathbf{r}}$

$$\boldsymbol{\Sigma}^{\mathbf{S}}_{\mathbf{r}} = \begin{bmatrix} 1 & 0 & 0 \\ 0 & 1 - r_0 & 0 \\ 0 & 0 & 0 \end{bmatrix} \tag{3.3}$$

where r_0 is the stress tensor aspect ratio

$$r_0 = \frac{\sigma_1 - \sigma_2}{\sigma_1 - \sigma_3} \tag{3.4}$$

The full stress tensor has 6 independent parameters:

- 3 principal stress magnitudes, $\sigma_1, \sigma_2, \sigma_3$, and
- 3 parameters that define the orientation of the principal stress directions, i.e., of the S frame.

The reduced stress tensor has only 4 independent parameters:

- the stress tensor aspect ratio, r_0, and
- 3 parameters that define the orientation of the principal stress directions, i.e., of the S frame.

Slip inversion constrains the reduced stress tensor only, but frictional analysis requires an extra parameter, s_0 (*Célérier*, 1988; *Tajima and Célérier*, 1989; *Burg et al.*, 2005; *Célérier et al.*, 2012):

$$s_0 = \frac{\sigma_1 - \sigma_3}{\sigma_1} \tag{3.5}$$

With this parameter, equation (3.1) can be recast as:

$$\widehat{\boldsymbol{\Sigma}} = \sigma_1 \cdot s_0 \cdot \widehat{\boldsymbol{\Sigma}}_{\mathbf{r}} + \sigma_3 \cdot \widehat{\mathbf{I}} \tag{3.6}$$

3.4 Principal stress directions parameters

The operation that transforms the geographical frame, G, into the principal stress frame, S, that are both right handed orthonormal frame, is therefore a rotation and thus depends on three parameters.

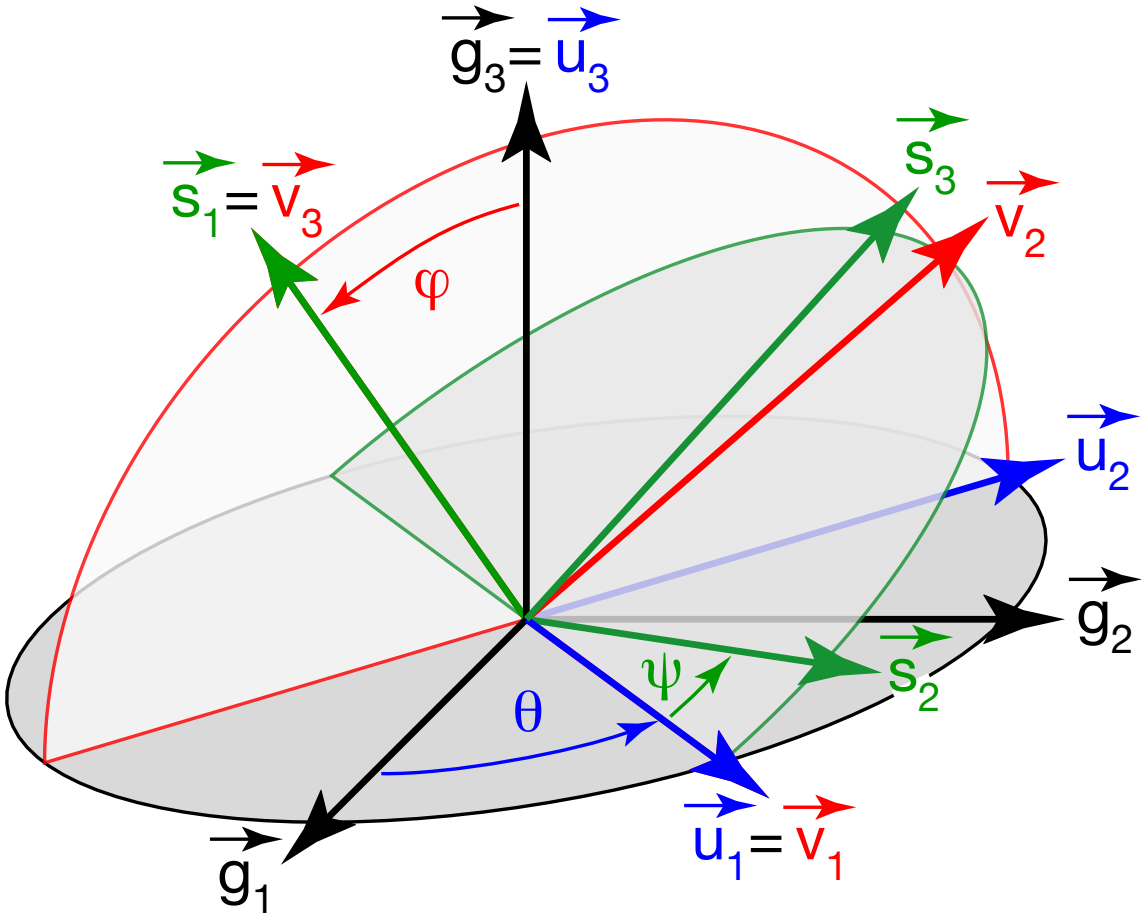

Figure 3.1: *Euler*'s (1767) angles transforming the geographical frame, $G = (\vec{g_1}, \vec{g_2}, \vec{g_3})$, into the principal stress frame, $S = (\vec{s_1}, \vec{s_2}, \vec{s_3})$, through 3 successive rotations of angles θ, φ, and ψ and axes $\vec{g_3}$, $\vec{u_1}$, and $\vec{s_1}$ (*Célérier*, 1988). The intermediate stages are $\vec{u_1}, \vec{u_2}, \vec{u_3}$ and $\vec{v_1}, \vec{v_2}, \vec{v_3}$.

3.4.1 Euler's angles

Euler introduced a powerful and elegant representation of the three independent parameters of a rotation by decomposing it into three successive elementary rotations (*Euler*, 1767). Following this idea, the global rotation that transforms G into S, can be decomposed into 3 elementary rotations of angles θ, φ, and ψ and axes $\vec{g_3}$, $\vec{u_1}$, and $\vec{s_1}$ (Fig. 3.1). The matrix $\mathbf{S^G}$ of this global rotation in the G frame, where the j^{th} column represents the coordinates of $\vec{s_j}$ in the G frame, becomes (*Célérier*, 1988):

$$\mathbf{S^G} = \begin{bmatrix} \sin\theta \cdot \sin\varphi & \cos\theta \cdot \cos\psi - \sin\theta \cdot \cos\varphi \cdot \sin\psi & -\cos\theta \cdot \sin\psi - \sin\theta \cdot \cos\varphi \cdot \cos\psi \\ -\cos\theta \cdot \sin\varphi & \sin\theta \cdot \cos\psi + \cos\theta \cdot \cos\varphi \cdot \sin\psi & -\sin\theta \cdot \sin\psi + \cos\theta \cdot \cos\varphi \cdot \cos\psi \\ \cos\varphi & \sin\varphi \cdot \sin\psi & \sin\varphi \cdot \cos\psi \end{bmatrix} \tag{3.7}$$

It is always possible to choose the S frame with two downgoing vectors, but not three, because of the constraint that it be right handed. Choosing downgoing $\vec{s_1}$ and $\vec{s_3}$ restrains the angles to:

- $\theta \in [0\,°, 360\,°]$
- $\varphi \in [0\,°, 90\,°]$
- $\psi \in]-90\,°, +90\,°]$

3.4.2 Trend and plunge angles

The principal stress directions are more usually represented by the trend and plunge of $\vec{s_1}$, $\vec{s_2}$, and $\vec{s_3}$. This representation is easier to interpret than Euler's angles. However, because the definition of S requires only 3 parameters, only 3 of the 6 trend and plunge parameters are independent. The angle ranges can be restricted to:

- Trend in $[0\,°, 360\,°]$
- Plunge in $[-90\,°, 90\,°]$

In geology directions are usually chosen downwards, so that plunge can be restricted to $[0\,°, 90\,°]$. This will be accepted in input.

However FSA internal representation transforms the input to build a right handed S frame with downgoing $\vec{s_1}$ and $\vec{s_3}$. Because of the requirement that the frame be right handed, $\vec{s_2}$ cannot be constrained to be downgoing. As a result the plunges $\vec{s_1}$ and $\vec{s_3}$ are within $[0\,°, 90\,°]$, but that of $\vec{s_2}$ is within $[-90\,°, 90\,°]$ and this is what will be found in output.

3.5 Stress data types

Data type defines the amount of information contained in the data and constrains the operations that the software will be allowed to do with these data. FSA can handle 6 data types that are listed in Table 3.1. Each data type is tagged in the software with an identification integer (ID) which given in the right column of Table 3.1.

For all types discussed below, only the reduced stress tensor, introduced in section 3.3 and equations 3.1 and 3.6, is involved. It is defined by r_0 (equation 3.4) and the principal stress directions, i.e., the orientation of the $S = (\vec{s_1}, \vec{s_2}, \vec{s_3})$ frame (section 3.2 and Table 1.1) with respect to the geographical frame, G (section 1.4 and Table 1.1). This orientation can be defined

- either by 3 Euler's angles that transform G into S (section 3.4.1 and Fig 3.1)
- or by the 6 trend and plunge angles of $\vec{s_1}$, $\vec{s_2}$, and $\vec{s_3}$ (section 3.4.2).

Table 3.1: Stress data types

Data types	ID
S by Euler's angles and r_0	200
S by Euler's angles, r_0, and 2 coordinates	202
S by Euler's angles, r_0, and 3 coordinates	203
S by azimuth and plunge and r_0	250
S by azimuth and plunge, r_0, and 2 coordinates	252
S by azimuth and plunge, r_0, and 3 coordinates	253

3.5.1 S by Euler's angles and r_0

Definition: Reduced stress tensor given by Euler's angles and r_0.

3.5.2 S by Euler's angles, r_0 and 2 coordinates

Definition: Reduced stress tensor given by Euler's angles and r_0 with 2 location coordinates. The coordinates can be either cartesian coordinates, x and y, in a frame of reference or spherical coordinates, longitude and latitude.

3.5.3 S by Euler's angles, r_0 and 3 coordinates

Definition: Reduced stress tensor given by Euler's angles and r_0 with 3 location coordinates. The coordinates can be either cartesian coordinates, x, y and z, in a frame of reference or spherical coordinates, longitude, latitude and depth.

3.5.4 S by azimuth and plunge and r_0

Definition: Reduced stress tensor given by the azimuth and plunge of the 3 principal stress directions $\vec{s_1}$,$\vec{s_2}$, and $\vec{s_3}$ and by r_0. Note that because the defintion of S requires only 3 parameters, only 3 of the 6 trend and plunge parameters are independent.

3.5.5 S by azimuth and plunge, r_0 and 2 coordinates

Definition: Reduced stress tensor given by the azimuth and plunge of the 3 principal stress directions $\vec{s_1}$,$\vec{s_2}$, and $\vec{s_3}$ and by r_0 with 2 location coordinates. The coordinates can be either cartesian coordinates, x and y, in a frame of reference or spherical coordinates, longitude and latitude.

3.5.6 S by azimuth and plunge, r_0 and 3 coordinates

Definition: Reduced stress tensor given by the azimuth and plunge of the 3 principal stress directions $\vec{s_1}$,$\vec{s_2}$, and $\vec{s_3}$ and by r_0 with 3 location coordinates. The coordinates can be either cartesian coordinates, x, y and z, in a frame of reference or spherical coordinates, longitude, latitude and depth.

Part III

Data files

Chapter 4

Fault and slip data files

4.1 Introduction

The goal of this chapter is to describe the format of fault and slip data input files accepted by Fsa.

Fsa has been designed to handle various types of fault and slip data since version 19, and 8 types are available for Fsa $\geq$ 35.4.

Morevover for each data type, the program can also handle various input file formats, some of them due to various ways of recording them. This results in 23 input file formats for Fsa versions $\geq$ 35.4, that are described below.

The correspondence between the 23 formats and 8 types is summarized in Table 4.1.

It is therefore necessary to set both data types and data format before reading any input file. As a consequence, three steps are required before reading an input file:

1. Specification of the data type
2. Specification of the data file format
3. Specification of the data file, i.e., its location and name.

Fault and slip data output files follow the same formats as input files, and can thus also be used as input. Conversion between formats can thus be achieved by reading data from an input file in one format and writing them into an output file in a different format.

4.2 Common conventions for all data files

The data files are Fortran sequential input files. They are ASCII text files containing character strings or numbers,. Further sequential files details and caveats are set out in Chapter 6.

The preferred layout, used in 16 formats, relies on FORTRAN free format and follows a standard file structure that begins with a standard header which is followed by standard data lines. The standard header contains two lines with a title in the first line and columns headers in the second line. File with this layout can be created in and then exported from text editors, spreadsheets, or word processors as detailed in section 6.4. They can also easily be imported in spreadsheets.

The remaining 7 formats use FORTRAN fixed format. Files with these formats can be created in and then exported from text editors, or word processors (Section 6.4).

Table 4.1: Fault slip data types and formats. ID = Data type identifier

Data types		Data formats		
Types	ID	Aki & Richards strike, dip, rake	Etchecopar strike, dip, pitch/trend	Dip direction, dip, trend, plunge
Fault and slip	100	SDR	EF EM	ADTP2I DAPT2I
Fault and slip with rake range	110	SDRH		
Fault and slip with bedding	150	SDRSD	EMB	
Original and restored fault and slip with bedding	200	2(SDR)SD		
Fault plane solution	300	SDR 2(SDR) CMT-dek-NP		
Fault plane solution and 3 coordinates	313	SDR3C 2(SDR)3C CMT-dek-NP CMT-ndk-NP FPFIT HASH		
Plane	400	SD	EFP EMP	DA
Plane and 1 coordinate	411	SDC		DAC GF-CDA

4.3 Formats using strike, dip, rake with Aki & Richards' convention

Here are grouped various formats that all represent fault and slip orientation by strike, dip, and rake with Aki & Richards' convention.

4.3.1 SDR: strike, dip, rake

- Purpose
  - For fault and slip data or one nodal plane of a fault plane solution.
- File structure
  - Standard file structure
- Data line structure
  - 3 real numbers in free format.
  - The 3 real numbers correspond to the strike, dip and rake in degrees with Aki & Richards' convention.
- Sample file
  - RD37_fs_sdr.txt

4.3.2 SD: strike, dip

- Purpose
  - For planar structure orientation data
- File structure
  - Standard file structure
- Data line structure
  - 2 real numbers in free format.
  - The 2 real numbers correspond to the strike and dip in degrees with Aki & Richards' convention.

4.3.3 SDC: strike, dip, z

- Purpose
  - For planar structure with 1 space coordinate orientation data
- File structure
  - Standard file structure
- Data line structure
  - 3 real numbers in free format.

  - The 3 real numbers correspond to the strike and dip in degrees with Aki & Richards' convention, and to the space coordinate, either distance along path (for outcrops) or depth (for boreholes).

4.3.4 SDR3C: strike, dip, rake, x, y, z

- Purpose
  - For fault plane solutions with 3 space coordinates
- File structure
  - Standard file structure
- Data line structure
  - 6 real numbers in free format.
  - The 6 real numbers correspond to strike, dip and rake in degrees with Aki & Richards' convention, and to the 3 space coordinates, (either x, y, z or longitude, latitude, depth)

4.3.5 2(SDR): 2•(strike, dip, rake)

- Purpose
  - For fault plane solutions where both nodal planes are given.
- File structure
  - Standard file structure
- Data line structure
  - 6 real numbers in free format.
  - The 6 real numbers correspond to the strike, dip and rake for the first nodal plane followed by the strike, dip and rake for the second nodal planes. Angles are in degrees and follow Aki & Richards' convention.

4.3.6 2(SDR)3c: 2•(strike, dip, rake), x, y, z

- Purpose
  - For fault plane solutions with 3 space coordinates where both nodal planes are given.
- File structure
  - Standard file structure
- Data line structure

  - 9 real numbers in free format.
  - The 9 real numbers correspond to strike, dip and rake for the first nodal planes, followed by those for the second nodal plane, followed by the 3 space coordinates (either x, y, z, or longitude, latitude, depth). Strike, dip and rake are in degrees and follow Aki & Richards' convention.

4.3.7 SDRSD: strike, dip, rake, strike, dip

- Purpose
  - For fault and slip with bedding orientation data. The bedding plane orientation is measured at the same location as the fault. This can then be used to restore the structural orientations to the situation where bedding is horizontal.
- File structure
  - Standard file structure
- Data line structure
  - 5 real numbers in free format.
  - The 5 real numbers correspond to the strike, dip and rake of the fault and slip data and to the strike and dip of the bedding. All angles are in degrees and Aki & Richards' convention is used

4.3.8 2(SDR)SD: 2•(strike, dip, rake), strike, dip

- Purpose
  - For original and restored fault and slip with bedding plane data. This format is used for output after restoration of the structural orientations to the situation with horizontal bedding.
- File structure
  - Standard file structure
- Data line structure
  - 8 real numbers in free format.
  - The 8 real numbers correspond to the strike, dip and rake of the original fault and slip data, to the strike, dip and rake of the restored fault and slip data, and to the strike, dip of the bedding. All angles are in degrees and Aki & Richards' convention is used.

4.3.9 SDRH: strike, dip, rake, half rake range

- Purpose
  - For fault and slip with rake range data.
- File structure
  - Standard file structure
- Data line structure
  - 4 real numbers in free format.
  - The 4 real numbers correspond to the strike, dip, rake, and half the uncertainty range in rake of the fault and slip data. All angles are in degrees and Aki & Richards' convention is used.
- Examples of rake ranges in Table 4.2.

Table 4.2: Rake uncertainty range

Observed constraint on		Rake range	Rake	Half rake range
strike slip sense	dip slip sense			
Senestral	None	[-90, 90]	0	90
None	Normal	[-180, 0]	-90	90
Senestral	Normal	[-90, 0]	-45	45

4.3.10 CMT-dek-NP

- Purpose
  - Older format of the Harvard Centroid Moment Tensor catalog.
  - Can be read either as fault plane solutions or as fault plane solutions with 3 coordinates.
  - For input of the nodal planes information with or without location, depending on the selected type.
- File structure
  1. No header.
  2. Data lines: each datum correspond to 4 lines.
- Data line structure
  - Parameters are read in fixed format described in the CMT-dek documentation

4.3.11 CMT-ndk-NP

- Purpose
  - Current format of the Global Centroid Moment Tensor catalog.
  - Read as fault plane solutions with 3 coordinates.
  - For input of the nodal planes and location information.
- File structure
  1. No header.
  2. Data lines: each datum correspond to 5 lines.
- Data line structure
  - Parameters are read in fixed format described in the CMT-ndk documentation

4.3.12 FPFIT

- Purpose
  - Ouput format of the FPFIT program (*Reasenberg and Oppenheimer*, 1985).
  - Read as fault plane solutions with 3 coordinates.
- File structure
  1. No header.
  2. Data lines: each datum correspond to 1 line.
- Data line structure
  - Parameters are read in fixed format described in the FPFIT documentation (*Reasenberg and Oppenheimer*, 1985).

4.3.13 HASH

- Purpose
  - Format of the SCEDC focal mechanism catalog for southern California (*Yang et al.*, 2012; *Hauksson et al.*, 2012).
  - Read as fault plane solutions with 3 coordinates.
- File structure
  1. No header.
  2. Data lines: each datum correspond to 1 line.
- Data line structure

  - Parameters are read in fixed format described in the SCEDC catalog.

4.4 Strike, dip, pitch/trend based on Etchecopar's Faille format

4.4.1 EF: original Etchecopar's Faille format

- Purpose
  - For field measurements of fault and slip data.
  - Combines strike, dip, pitch and strike, dip, trend field measurements into a single data file.
  - Sole format accepted by Etchecopar & Vasseur's program, FAILLE (*Etchecopar et al.*, 1981; *Etchecopar*, 1984).
  - Useful for legacy data.
- File structure
  1. Non standard single line header: the first line contains the title, read in fixed format.
  2. Data lines: each datum correspond to 1 line.
  3. The last line has number 450 in column 3-4-5, i.e. at the location of strike (Table 4.3), to indicate the end of data.
- Data line structure
  - each data line is
    - either of the type
      (strike, dip, dip quadrant, rake, rake quadrant, fault type, id)
    - or of the type
      (strike, dip, dip quadrant, slip trend, fault type, id).
  - The data lines are read in Fortran fixed format:
    FORMAT (T3,I3,T10,I2,T17,A1,T21,I2,T26,A1,T29,I3,T35,A1,T70,I3,T74,1A3).
    This implies that character strings are not delimited by quotes, but by their column location
  - Parameters and their positions are described in Table 4.3 .
- Sample file
  - RD37_fs_ef.txt

Table 4.3: EF format data line: Etchecopar's FAILLE format.

Data	Type	Range	Comment	Column location[1]
strike	integer	[0, 360]	strike azimuth[2]	3-4-5
dip	integer	[0, 90]	dip angle[2]	10-11
dip quadrant	character	{N, E, S, W}	dip quadrant[3]	17
rake	integer	[0, 90]	rake or pitch angle[2,5]	21-22
rake quadrant	character	{N, E, S, W}	rake quadrant[3,5]	26
slip azimuth	integer	[0, 180]	slip azimuth[2,5]	29-30-31
fault type	character	{N, I, D, S}	fault type[4]	35
id	integer	[0, 999]	identifies the fault	70-71-72

[1] Column location here refers to the character position in the 80 characters line (col 1 to 80 for a data line: old punch card format).
[2] Angles are integers and in degrees.
[3] N, E, S, W are upper case, single character variables. N, E, S, W = North, East, South, West.
[4] N, I, D, S are upper case, single character variables. N, I, D, S = Normal, Reverse (Inverse), Dextral, Sinistral.
[5] In FSA, if the rake quadrant string is blank (i.e., rake quadrant = ' ') and rake = 0, then slip azimuth is used. In FAILLE this test is reversed: if slip azimuth = 0 (or blank space) then rake is used: thus an azimuth = 0 slip is wrongly assumed to be a pitch = 0 slip. Conclusion: to avoid this problem when using FAILLE, replace azimuth = 0 by azimuth = 180.

4.4.2 EFP: original Etchecopar's Faille for plane only

- Purpose
  - Similar to format EF, but for plane only data.
- File structure
  - Same as EF.
- Data line structure
  - Same as EF, with the same position, but only (strike, dip, dip quadrant, id) are filled. Other parameters filled with blank spaces.

4.4.3 EM: Modified Etchecopar

- Purpose
  - For field measurements of fault and slip data.
  - This format is a modification of the Etchecopar's original EF format that

    - allows to prepare the data file in a spreadsheet,
    - is read in free format,
    - avoids the slip rake versus slip azimuth ambiguity,
    - but still corresponds closely to field measurements.

- File structure
  - Standard file structure
- Data line structure
  - Data lines are made of 3 real numbers, one integer number, and 3 character strings.
  - The data lines are read in Fortran free format.
  - Each data line lists the following parameters in this order:
    strike, dip, dip quadrant, slip angle, slip quadrant, fault type, id.
  - Parameters are described in Table 4.4 .
- The data file can be prepared in a spreadsheet as follow:
  1. enter the data in a spreadsheet;
  2. save them as a text file;
  3. open the text file in a text editor or word processor and replace all occurrences of N, E, S, W, A, I, D by 'N', 'E', 'S', 'W', 'A', 'I', 'D';
  4. save again as text;
  5. verify end of line and end of file and alter them if needed (most easily done with a text editor);
  6. save again as text: this is the input file.
- Sample file
  - RD37_fs_em.txt

4.4.4 EMP: Modified Etchecopar for plane only

- Purpose
  - Similar to format EM, but for planar structure orientation data.
- File structure
  - Standard file structure
- Data line structure

- Data lines are made of 2 real numbers, one integer number, and 1 character strings.
- The data lines are read in Fortran free format.
- Each data line lists the following parameters in this order:
  strike, dip, dip quadrant, id.
- Parameters are described in Table 4.5 .

Table 4.4: EM format data line: modified Etchecopar.

Data	Type	Range	Comment	Column number[1]
strike	real	[0, 360]	strike azimuth[2]	1
dip	real	[0, 90]	dip angle[2]	2
dip quadrant	character	{N, E, S, W}	dip quadrant[3]	3
slip angle	real	[0, 180]	slip angle[2]	4
slip quadrant	character	{N, E, S, W, A}	rake quadrant[3] or azimuth tag[5]	5
fault type	character	{N, I, D, S}	fault type[4]	6
id	integer	[0, 999]	identifies the fault	7

[1] Columns number here refer to spreadsheet columns, i.e., to the tab-separated entries in the text file.
[2] Angles are real numbers and in degrees.
[3] N, E, S, W are upper case, single character variables. N, E, S, W = North, East, South, West.
[4] N, I, D, S are upper case, single character variables. N, I, D, S = Normal, Reverse (Inverse), Dextral, Sinistral.
[5] Slip angle interpretation: if slip quadrant $\in$ {N, E, S, W}, then slip angle is the rake within [0,90]; if slip quadrant = A, then slip angle is the slip azimuth within [0,180].

Table 4.5: EMP format data line: modified Etchecopar for plane only.
Same conventions as in Table 4.4.

Data	Type	Range	Comment	Column number
strike	real	[0, 360]	strike azimuth	1
dip	real	[0, 90]	dip angle	2
dip quadrant	character	{N, E, S, W}	dip quadrant	3
id	integer	[0, 999]	identifies the fault	4

4.4.5 EMB: Modified Etchecopar for fault slip with bedding

- Purpose
  - Similar to format EM, but for fault and slip with bedding orientation data.
- File structure
  - Standard file structure
- Data line structure
  - Data lines are made of 5 real numbers, one integer number, and 4 character strings.
  - The data lines are read in Fortran free format.
  - Each data line lists the following parameters in this order:
    strike, dip, dip quadrant, slip angle, slip quadrant, fault type, id, bedding strike, bedding dip, bedding dip quadrant.
  - Parameters are described in Table 4.6 .

Table 4.6: EMB format data line: modified Etchecopar for fault slip with bedding. Same conventions as in Table 4.4.

Data	Type	Range	Comment	Column number
strike	real	[0, 360]	strike azimuth	1
dip	real	[0, 90]	dip angle	2
dip quadrant	character	{N, E, S, W}	dip quadrant	3
slip angle	real	[0, 180]	slip angle	4
slip quadrant	character	{N, E, S, W, A}	rake quadrant or azimuth tag	5
fault type	character	{N, I, D, S}	fault type	6
id	integer	[0, 999]	identifies the fault	7
bedding strike	real	[0, 360]	strike azimuth	8
bedding dip	real	[0, 90]	dip angle	9
bedding dip quadrant	character	{N, E, S, W}	dip quadrant	10

4.5 Dip direction, dip, trend, plunge formats

In these input formats where slip orientation is given by trend and plunge, measurements errors will usually place the slip vector slightly out of the fault plane. Rake is therefore computed by projecting the slip vector on the fault plane either vertically for low dip planes or horizontally for high dip planes. The FSA program also computes the angle, β, between slip vector and fault plane and issues

- a warning when $3\,^\circ \leq \beta < 10\,^\circ$ and
- an error message when $10\,^\circ \leq \beta$

4.5.1 DA: dip, dip direction

- Purpose
  - For planar structure orientation data.
  - Concise, fully numerical and unambiguous.
- File structure
  - Standard file structure
- Data line structure
  - 2 real numbers in free format.
  - The 2 real numbers correspond to the dip and dip direction in degrees.

4.5.2 DAC: dip, dip direction, z

- Purpose
  - For plane and 1 coordinate data.
  - Concise, fully numerical and unambiguous.
- File structure
  - Standard file structure
- Data line structure
  - 3 real numbers in free format.
  - The 3 real numbers correspond to the dip and dip direction in degrees, and to the space coordinate.

4.5.3 GF-CDA: Geoframe z, dip, dip direction

- Purpose
  - Format of the dip to ASCII output file of Schlumberger Geoframe planar structure picks.
- File structure
  1. No header.
  2. Data lines: each datum correspond to 1 line.

- Data line structure
  - Parameters are read in fixed format.
  - Only the depth, dip and dip direction are read.

4.5.4 ADTP2I: Dip direction, dip, trend, plunge

- Purpose
  - For fault and slip data where slip direction is given by trend and plunge.
- File structure
  - Standard file structure
- Data line structure
  - 6 numbers in free format: 4 real numbers followed by 2 integer numbers.
  - The 6 numbers are read in free format and are ordered as follows :
    1. the fault plane dip direction in degrees (real number)
    2. the fault plane dip angle in degrees (real number)
    3. the slip vector trend (azimuth) in degrees (real number)
    4. the slip vector plunge in degrees (real number)
    5. a code within [1,4] for the movement type:
       1 = reverse, 2 = normal, 3 = dextral, 4 = sinistral (integer number)
    6. an identification number for the datum (integer number)

4.5.5 DAPT2I: Dip, dip direction, plunge, trend

- Purpose
  - For fault and slip data where slip direction is given by trend and plunge.
  - Same as ADTP2I, but with different order in the data line
- File structure
  - Standard file structure
- Data line structure
  - Data lines are made of 6 numbers per data line in free format: 4 real numbers followed by 2 integer numbers.
  - The 6 numbers are read in free format and are ordered as follows :
    1. the fault plane dip angle in degrees (real number)

2. the fault plane dip direction in degrees (real number)
3. the slip vector plunge in degrees (real number)
4. the slip vector trend (azimuth) in degrees (real number)
5. a code within [1,4] for the movement type:
   1 = reverse, 2 = normal, 3 = dextral, 4 = sinistral (integer number)
6. an identification number for the datum (integer number)

Chapter 5

Stress data files

5.1 Introduction

The goal of this chapter is to describe the format of stress data input files accepted by FSA.

FSA can handle 6 types of stress data.

Morevover for each data type, the program can also handle various input file formats, some of them due to various ways of recording them. This results in 10 input file formats for FSA versions ≥ 32.2, that are described below.

The correspondence between the 10 formats and 6 types is summarized in Table 5.1.

It is therefore necessary to set both data types and data format before reading any input file. As a consequence, three steps are required before reading an input file:

1. Specification of the data type
2. Specification of the data file format
3. Specification of the data file, i.e., its location and name.

Stress data output files follow the same formats as input files, and can thus also be used as input. Conversion between formats can thus be achieved by reading data from an input file in one format and writing them into an output file in a different format.

5.2 Common conventions for all data files

The data files are FORTRAN sequential input files. They are ASCII text files containing character strings or numbers,. Further sequential files details and caveats are set out in Chapter 6.

Table 5.1: Stress data types and formats

Data types	ID	Data formats
S by Euler's angles and r_0	200	3ER
S by Euler's angles, r_0, and 2 coordinates	202	3ER2C
S by Euler's angles, r_0, and 3 coordinates	203	3ER3C
S by azimuth and plunge and r_0	250	3(AP)R 2(AP)-PT
S by azimuth and plunge, r_0, and 2 coordinates	252	3(AP)R2C
S by azimuth and plunge, r_0, and 3 coordinates	253	3(AP)R3C CMT-dek-PBT CMT-ndk-PBT 2(AP)3C-PT

The preferred layout, used in 8 formats, relies on FORTRAN free format and follows a standard file structure that begins with a standard header which is followed by standard data lines. The standard header contains two lines with a title in the first line and columns headers in the second line. File with this layout can be created in and then exported from text editors, spreadsheets, or word processors as detailed in section 6.4. They can also easily be imported in spreadsheets.

The remaining 2 formats use FORTRAN fixed format. Files with these formats can be created in and then exported from text editors, or word processors (Section 6.4).

5.3 Euler's angles formats

Here are grouped various formats that use Euler's angles to define principal stress directions.

5.3.1 3ER: three Euler's angles and r_0

- Purpose
  - For reduced stress tensor data given by Euler's angles and r_0.
- File structure
  - Standard file structure
- Data line structure
  - 4 real numbers in Fortran free format.
  - The 4 real numbers correspond to three Euler's angles θ, φ, ψ, and the ratio r_0. Angles are in degrees
- Sample file

  - sv_st_3er.txt

5.3.2 3ER2C: three Euler's angles, r_0, and 2 coordinates

- Purpose
  - For reduced stress tensor data given by Euler's angles, r_0, and 2 coordinates for location.
  - This format is obsolescent and the similar format with 3 coordinates should be used instead.
- File structure
  - Standard file structure
- Data line structure
  - 6 real numbers in Fortran free format.
  - The 6 real numbers correspond to three Euler's angles, θ, φ, ψ, the ratio r_0, and the two coordinates: either x, y or longitude, latitude. Angles are in degrees

5.3.3 3ER3C: three Euler's angles, r_0, and 3 coordinates

- Purpose
  - For reduced stress tensor data given by Euler's angles, r_0, and 3 coordinates for location.
- File structure
  - Standard file structure
- Data line structure
  - 7 real numbers in Fortran free format.
  - The 7 real numbers correspond to three Euler's angles, θ, φ, ψ, the ratio r_0, and the three coordinates: either x, y, z or longitude, latitude, depth. Angles are in degrees

5.4 Azimuth and plunge formats

Here are grouped various formats that use azimuth and plunge to define the principal stress directions.

5.4.1 3(AP)R: 3•(azimuth, plunge), r_0

- Purpose
  - For reduced stress tensor data given by azimuth, plunge and r_0.
- File structure
  - Standard file structure
- Data line structure
  - 7 real numbers in Fortran free format.
  - The 7 real numbers correspond to the azimuth, plunge of $\vec{s_1}$, followed by the azimuth, plunge of $\vec{s_2}$ and $\vec{s_3}$, and the ratio r_0. Angles are in degrees.
- Sample file
  - sv_st_3(ap)r.txt

5.4.2 3(AP)R2C: 3•(azimuth, plunge), r_0 and 2 coordinates

- Purpose
  - For reduced stress tensor data given by azimuth, plunge, r_0, and 2 coordinates.
  - This format is obsolescent and the similar format with 3 coordinates should be used instead.
- File structure
  - Standard file structure
- Data line structure
  - 9 real numbers in Fortran free format.
  - The 9 real numbers correspond to the azimuth, plunge of $\vec{s_1}$, $\vec{s_2}$, $\vec{s_3}$, the ratio r_0, and the two coordinates: either x, y or longitude, latitude. Angles are in degrees

5.4.3 3(AP)R3C: 3•(azimuth, plunge), r_0 and 3 coordinates

- Purpose
  - For reduced stress tensor data given by azimuth, plunge, r_0, and 3 coordinates.
- File structure
  - Standard file structure
- Data line structure

  - 10 real numbers in Fortran free format.
  - The 10 real numbers correspond to the azimuth, plunge of $\vec{s_1}$, $\vec{s_2}$, $\vec{s_3}$, the ratio r_0, and the three coordinates: either x, y, z or longitude, latitude, depth. Angles are in degrees

5.4.4 2(AP)-PT: 2•(azimuth, plunge)

- Purpose
  - For seismic catalog where only P and T axes are given. The two axes are completed with B to build S, and with an arbitrary r_0 to build a reduced stress tensor of azimuth, plunge, r_0 type.
- File structure
  - Standard file structure
- Data line structure
  - 4 real numbers in Fortran free format.
  - The 4 real numbers correspond to the azimuth, plunge of P, followed by the azimuth, plunge of T. Angles are in degrees

5.4.5 2(AP)3C-PT: 2•(azimuth, plunge) and 3 coordinates

- Purpose
  - For seismic catalog where only P and T axes are given with 3 coordinates. The two axes are completed with B to build S, and an arbitrary r_0 is added, to build a reduced stress tensor of azimuth and plunge, r_0 and 3 coordinates type.
- File structure
  - Standard file structure
- Data line structure
  - 7 real numbers in Fortran free format.
  - The 7 real numbers correspond to the azimuth, plunge of P, and T, and the three coordinates: either x, y, z or longitude, latitude, depth. Angles are in degrees.

5.4.6 CMT-dek-PBT

- Purpose
  - Older format of the Harvard Centroid Moment Tensor catalog.

  - P, B and T are read from the input file to build S, and an arbitrary value for r_0 is generated to build a reduced stress tensor of azimuth, plunge, r_0, and 3 coordinates type.

- File structure
  1. No header.
  2. Data lines: each datum correspond to 4 lines.
- Data line structure
  - Parameters are read in Fortran fixed format described in the CMT-dek documentation

5.4.7 CMT-ndk-PBT

- Purpose
  - Current format of the Global Centroid Moment Tensor catalog.
  - P, B and T are read from the input file to build S, and an arbitrary value for r_0 is generated to build a reduced stress tensor of azimuth, plunge, r_0, and 3 coordinates type.
- File structure
  1. No header.
  2. Data lines: each datum correspond to 5 lines.
- Data line structure
  - Parameters are read in Fortran fixed format described in the CMT-ndk documentation

Chapter 6

Fortran sequential files

6.1 Introduction

This chapter describes a few common attributes of sequential files used as input for or output from FORTRAN programs.

6.2 Fortran input/output sequential files

- Input or output sequential files are ASCII files, i.e. plain text files without accentuated characters. If input files are prepared within a software other than a pure text editor, such as a word processor or a spreadsheet, they need be exported as text only files.
- During input, each reading statement normally focusses on one input line with the following conventions:
  - if all the data to be read within a line are found, the rest of the line is not read; the next input statement will seek its data in the next line; this implies that extra information can be added AFTER the required data without affecting the input;
  - if all the data to be read are not found within a line, the missing data will be sought in the next line; this implies that an incomplete line will be completed by the probably misinterpreted next line.
- There are two possible formats for FORTRAN sequential files: free or fixed formats.

6.2.1 Fortran free format

- Input reading rules:
  - numbers must be delimited by empty spaces or tabulations;

  - character strings must be delimited by single quotes, ', to be read properly.

- Possible file preparation:
  - in a text editor, spreadsheet, or word processor, and saved as text only;
  - saving as tab separated text is most convenient, as it is easily exchanged with spreadsheets.

Free format is preferred and used as much as possible for input, not only because it is insensitive to exact data placement in the line (it is only sensitive to data order sequence and delimiters), which avoids many causes of input error, but also because it can easily be exchanged with spreadsheets.

6.2.2 Fortran fixed format

- Input reading rules:
  - numbers and character strings are read within a specific column location; column here meaning the number of characters (or spaces) counted from the beginning of the line;
  - no delimiters are necessary: character strings or numbers are delimited by their column location;
  - a column offset in a data line will result in misinterpreted data; for instance, if '1234' or 'abcd' are offset by one column to the left, they will be read in input as '2340' and 'bcd '.
- Possible file preparation:
  - in a text editor (recommended) or a word processor and saved as text only; each character or digit position must be counted from the beginning of each line.

Fixed format thus does not tolerate errors in data placement in the line, but does not require delimiters, which make it convenient in some circonstances.

6.3 Operating system issues

6.3.1 Encoding

Only ASCII characters are accepted in input, and the text encoding must be compatible with it. Best choice on recent systems is UTF-8, but many older encodings are also compatible, such as Mac OS Roman, Windows-1252, and Latin-1. Compatible encoding is usually achieved when saving as a plain text file from a text editor, a word processor, or a spreadsheet, and can be verified and modified in text editors.

6.3.2 End of line

The special character used to mark the end of line (EOL) in the input file must be consistent with the system used to run the software (Table 6.1). If the end of line is not recognized, the whole input file may appear as a single line to the program. Problems tend to arise when the file is transferred from one operating system to another, or when the file is exported from a word processor or spreadsheet. If ftp is used between systems, setting text, instead of binary, transfer of data files should translate the end of line.

It is therefore recommended to use a text editor to check, and eventually correct, end of line characteristics of data files that have been exchanged between systems or that have been exported from a word processor or a spreadsheet.

Table 6.1: End of line (EOL) coding in common operating systems.

Operating system	EOL symbol	EOL description
MacOS X	LF	Line Feed
Unix	LF	Line Feed
Windows	CRLF	Carriage Return + Line Feed
MacOS Classic	CR	Carriage Return

6.3.3 End of file

- Aways terminate the file with an empty line (extra line with no space). This avoids putting the end of file (EOF) tag in the last data line. In some systems, including MacOS X, such a situation can result in the last data line not being read.
- Always check that the number of data stored in the program is exactly the expected number of data. If one datum is missing, the above most likely applies.

6.4 Creating input files

Input files can be created with a text editor (recommended) or exported from a word processor. Free format data files can also be exported from a spreadsheet.

6.4.1 Text editors

Preparing an input file with a text editor has the advantage of directly creating a plain text file. There then only remain two issues to deal with when saving the file:

1. check and eventually modify end of line coding, and
2. make sure the end of file is below the last data line.

Here are a few text editors that allow to verify and alter end of line and text encoding of text files:

- under MacOS X: TextWrangler, BBEdit, Smultron, and Plain Text Editor;
- under Windows: ConTEXT.

6.4.2 Spreadsheets

Input files that are read in free format can be exported from spreadsheet. There are then four issues to deal with:

1. exporting the file as tab delimited text,
2. making sure that character strings are enclosed within quotes,
3. checking and eventually correcting end of line coding, and
4. making sure the end of file is below the last data line.

The last three issues are best dealt with by importing the file into a text editor.

6.4.3 Word processors

Finally, input files can also be exported from a word processor. Three issues must be dealt with:

1. exporting the file in plain text (tab delimited columns recommended),
2. checking and eventually correcting end of line coding, and
3. making sure the end of file is below the last data line.

Again, the last two issues are best dealt with by importing the file into a text editor.

6.5 Standard input/output files

A file format designed to be easily exchanged with spreadsheets is called 'standard file' in this documents and used as much as possible by the software.

6.5.1 Standard file structure

- Data files are ASCII files.
- They are made of a header followed by data lines.

6.5.2 Standard header

The standard header is made of two lines:

1. Title line: the first line contains the title.
2. Columns headers line: the second line contains the columns headers

The standard header is read in free format: title and column headers are character strings and need be delimited by single quotes ', so as to be read properly.

6.5.3 Standard data line

- All parameters for each datum are given in a single data line.
- Data line are read in free format. Parameters may be separated by empty spaces or tabs. Character strings need be delimited by single quotes '.

6.5.4 Standard file example

Example of a standard data file with 2 reals, 1 integer and 1 character string per data. Here are the 3 first lines of the file with two header lines and the first data line:

1. 'Title'
2. 'Parameter-1' 'Parameter-2' 'Parameter-3' 'Parameter-4'
3. 12000.6 2999.4567 245 'label-of-data1'

Part IV

Procedures

Chapter 7

Procedures: introduction

Procedures are organized into 5 categories.

1. Procedures concerning fault slip data only:
   - Fault slip data analysis (Chapter 8);
   - Generating synthetic fault slip data.
2. Procedures concerning stress data only:
   - Stress data analysis (Chapter 9);
   - Generating synthetic stress data.
3. Procedures using fault slip data to generate stress data:
   - Optimal stress (Section 10.2);
   - P, B, and T axes (Section 10.3);
   - Stress inversion (Chapter 11).
4. Procedures using stress data to generate fault slip data:
   - Generating conjugate planes from principal stress orientations;
   - Generating nodal planes from P, B, and T axes.
5. Procedures using stress and fault slip data:
   - Analysis of the relationship between fault slip and stress (Chapter 12).

Chapter 8

Fault slip data analysis

8.1 Introduction

This chapter lists procedures that analyse fault slip data without affecting stress data.

8.2 Input and output of fault slip data

8.2.1 Input of fault slip data

Data types are described in Section 2.4 and Table 2.2, while accepted file formats are described in Chapter 4 and Table 4.1.

8.2.2 Output of fault slip data

Most input file formats can also be used as output file formats, so that the output format does not have to be identical to the input format, provided it remains compatible with the data type as described in Table 4.1. The output routine thus allows to use any of the formats that are compatible with the loaded data type.

8.2.3 Conversion between formats

Conversion between file formats for a given data type can be achieved by reading data files in the source format and writing them in the target format.

8.3 Graphical representation of fault slip data

8.3.1 Stereographic projection

Stereographic projection can be

- either equal area (*Schmidt*, 1925) (default),
- or conformal (*Wulff*, 1902).

and can plot

- planes and slip vectors
- poles of planes
- slip vectors

8.3.2 Statistics

Statistics can be computed for

- strike
- dip
- rake
- trend
- plunge

and can be represented

- either as histograms (default),
- or as roses

8.3.3 Breddin's graph

A rake versus strike plot can also be produced. It is designed to be overlain by Breddin's graph, to graphically assess the tectonic regime (*Célérier and Séranne*, 2001). Abaci at the same scale as these plots are available at
`http://www.celerier.gm.univ-montp2.fr/rsch/breddin/breddin.html`.

8.3.4 Mapping fault and slip data

Mapping is available for data with geographical coordinates.

8.4 Restoring structures to horizontal bedding

When fault slip data are recorded with bedding orientation as fault and slip with bedding data type, then it becomes possible to apply a rotation of angle equal to the dip angle and with axis along the strike direction to restore the structures to the situation where bedding is horizontal. Both original and rotated data can then be exported in an output file of format 2(SDR)SD.

Chapter 9

Stress data analysis

9.1 Introduction

This chapter lists procedures that analyse stress data without affecting fault slip data.

9.2 Input and output of stress data data

9.2.1 Input of stress data

Data types are described in Section 3.5 and Table 3.1, while accepted file formats are described in Chapter 5 and Table 5.1.

9.2.2 Output of stress data

Most input file formats can also be used as output file formats, so that the output format does not have to be identical to the input format, provided it remains compatible with the data type as described in Table 5.1. The output routine thus allows to use any of the formats that are compatible with the loaded data type.

9.2.3 Conversion between formats

Conversion between file formats for a given data type can be achieved by reading data files in the source format and writing them in the target format.

9.3 Graphical representation of stress data

9.3.1 Stereographic projection

Principal stress directions $\vec{s_1}, \vec{s_2}, \vec{s_3}$ can be plotted on a stereographic projection that can be

- either equal area (*Schmidt*, 1925) (default),
- or conformal (*Wulff*, 1902).

9.3.2 Statistics

Statistics can be computed for

- trends of $\vec{s_1}, \vec{s_2}, \vec{s_3}$
- plunges of $\vec{s_1}, \vec{s_2}, \vec{s_3}$

and can be represented

- either as histograms (default),
- or as roses

9.3.3 Tectonic regime diagram

Tectonic regime, originally defined by the principal stress orientations (*Anderson*, 1905, 2012, 1951; *Bucher*, 1920, 1921; *Harland and Bayly*, 1958), has been extended to include the stress tensor aspect ratio (*Armijo et al.*, 1982; *Philip*, 1987; *Guiraud et al.*, 1989; *Tajima and Célérier*, 1989). Reduced stress tensors can be plotted in a tectonic regime diagram that follows that of *Célérier* (1995).

9.3.4 Triangular diagram

Principal stress orientations $\vec{s_1}, \vec{s_2}, \vec{s_3}$ can also be represented in a triangular diagram introduced by *Frohlich and Apperson* (1992) and *Frohlich* (1992, 2001). This is achieved by replacing P, B, T by $\vec{s_1}, \vec{s_2}, \vec{s_3}$. Because the $S = (\vec{s_1}, \vec{s_2}, \vec{s_3})$ frame is right handed, the resulting triangular diagram is a mirror of the original proposition along a vertical axis (*Célérier*, 2008, 2010).

The projection can be set

- either as gnomonic (default) (*Frohlich and Apperson*, 1992; *Frohlich*, 1992, 2001),
- or as Lambert azimuthal equal area (*Kaverina et al.*, 1996).

9.3.5 Mapping stress data

Mapping is available for data with geographical coordinates.

Chapter 10

Optimal Stress

10.1 Introduction

Early, and probably earliest, attempts to relate fault slip to causing stress compared conjugate faults observed in nature with those obtained in material testing by engineers where the stress system is known. This allowed to infer principal stress orientations from conjugate faults (*Hoskins*, 1896; *Van Hise*, 1896; *Anderson*, 1905, 2012, 1951; *Bucher*, 1920, 1921; *Hubbert*, 1951, 1972). This approach was then extended to a single fault where the slip orientation is known (*Friedman*, 1964; *Compton*, 1966; *Etchecopar*, 1984; *Huang and Angelier*, 1987, 1989).

10.2 Optimal principal stress directions

Given the friction angle ϕ_0 (Table 1.1) and defining

$$\phi_2 = 45^\circ - \phi_0/2 \tag{10.1}$$

the optimal principal stress frame $S = (\vec{s_1}, \vec{s_2}, \vec{s_3})$ is obtained by rotating the fault and slip frame $E = (\vec{e_1}, \vec{e_2}, \vec{e_3})$ by an angle ϕ_2 around $-\vec{e_2}$ (Fig. 10.4). This orientation is called optimal because iy is the the most favorable for fault reactivation.

10.3 P, B, T axes

Similarly, the P, B, T right handed frame $\left(\vec{p}, \vec{b}, \vec{t}\right)$ is obtained by rotating the fault and slip frame $E = (\vec{e_1}, \vec{e_2}, \vec{e_3})$ by an angle 45° around $-\vec{e_2}$ (Fig. 10.4).

10.4 Implementation

The required input is fault and slip data.

This approach yields one reduced stress tensor for each fault slip datum, so that the output is a set of $N_{st} = N_{fs}$ reduced stress tensors.

The stress tensor aspect ratio, r_0, is unconstrained and is assigned an arbitrary value to obtain a reduced tensor; this value is set as $r_0 = 0.5$ by default, but can be modified.

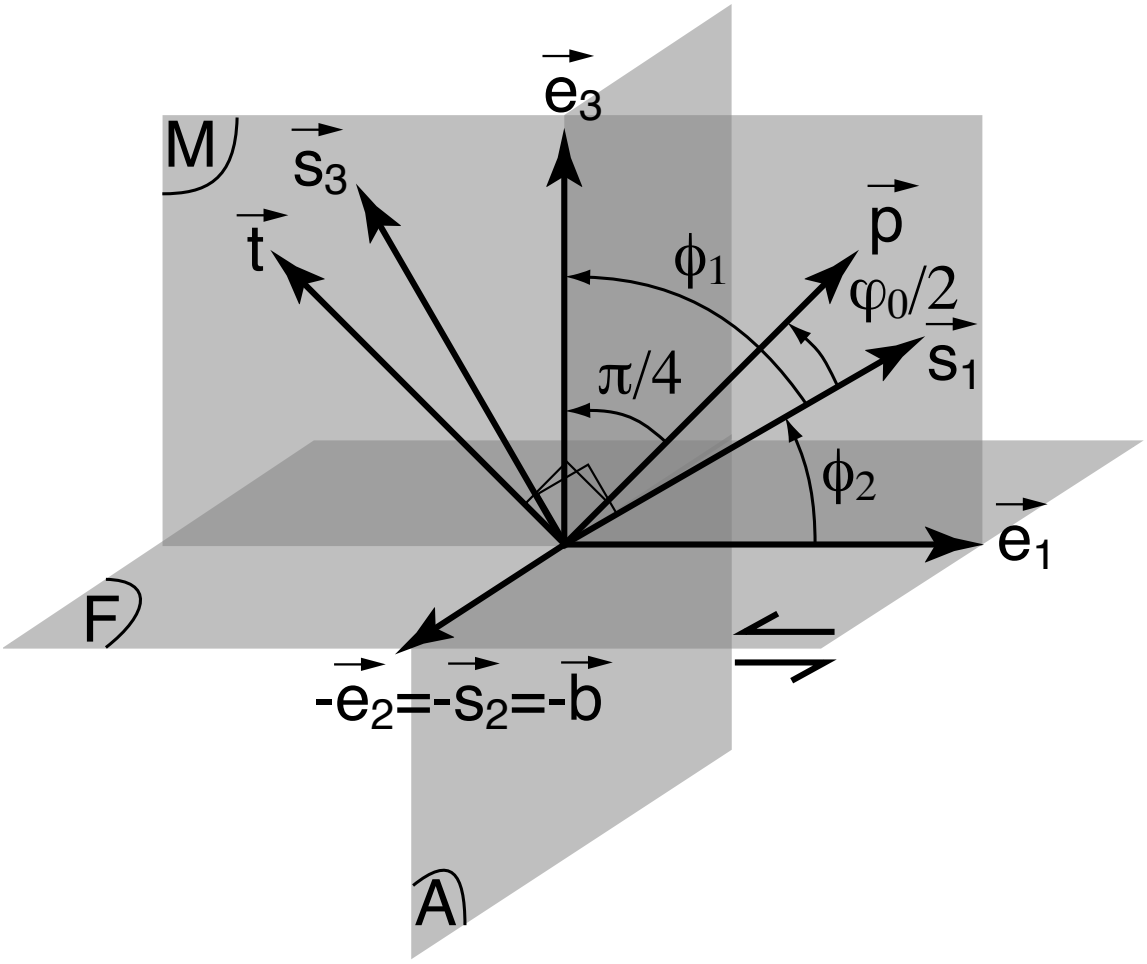

Figure 10.1: Optimal principal stress orientations, $S = (\vec{s_1}, \vec{s_2}, \vec{s_3})$, deduced from a fault plane, F, of normal $\vec{e_3}$ and slip direction $\vec{e_1}$. The plane of movement (*Arthaud*, 1969) is labeled M. ϕ_0 is the angle of internal friction, $\phi_1 = 45° + \phi_0/2$, and $\phi_2 = 45° - \phi_0/2$. Right handed frame of unit vectors $(\vec{p}, \vec{b}, \vec{t})$ along the P, B, T seismological axes of an earthquake focal mechanism with nodal planes F and A. $-\vec{e_2}$, $-\vec{s_2}$, and $-\vec{b}$ are shown instead of $\vec{e_2}$, $\vec{s_2}$, and $\vec{b}$ for the sake of clarity. Modified after *Célérier et al.* (2012).

Chapter 11

Stress inversion

11.1 Introduction

The compatiblity of a reduced stress tensor with index j, $\widehat{\mathbf{\Sigma}}_{\mathbf{r}j}$, with a fault slip datum of index i, is measured by an individual misfit, $m(i,j)$ (inversion parameters are summarized in Table 11.1).

Likewise, the compatibility of the same reduced stress tensor with a set of fault slip data is measured by a global misfit function, $M_F(j)$, that is derived from the individual misfits, $m(i,j)$.

The goal of stress inversion is to find a number, N_{st0}, of stress tensor solutions that minimize $M_F(j)$ among a population of N_{st} tested stress tensors.

The required input is fault and slip data. The output is a set of N_{st0} reduced stress tensors. By default $N_{st0} = 5$ but can be adjusted.

11.2 Misfit function

11.2.1 Misfit function options

The inversion process may be tuned in two ways.

First, the individual misfits may be adapted to deal with

- fault planes,
- or earthquake focal mechanisms with two nodal planes and where either may be the actual fault plane,

or to take into account 3 types of input uncertainties

- datum with a well defined slip rake (classical inversion),

- datum where rake of slip is defined within a range,
- datum where only strike or dip sense of slip is defined.

Second, the global misfit may be computed from

- all data or
- ony part of the data,

and can be set as

- the average of individual misfits or
- the maximum of individual misfits.

11.2.2 Individual misfit

We first consider the difference, $\Delta\lambda_{ij}$, between predicted, λ_{ij}^P, and measured, λ_i^M, rake for a fault slip datum of index i and a stress tensor of index j:

$$\Delta\lambda_{ij} = \lambda_{ij}^P - \lambda_i^M \tag{11.1}$$

We further constrain $\Delta\lambda_{ij}$ to satisfy

$$\Delta\lambda_{ij} \in [-180°, +180°] \tag{11.2}$$

We then define the rake difference, $D\lambda_{ij}$, for the i$^{\text{th}}$ fault slip datum and j$^{\text{th}}$ stress datum, as the absolute value of $\Delta\lambda_{ij}$:

$$D\lambda_{ij} = |\Delta\lambda_{ij}| \quad D\lambda_{ij} \in [0°, 180°] \tag{11.3}$$

The individual misfit, $m(i,j)$, for the i$^{\text{th}}$ fault slip datum and j$^{\text{th}}$ stress datum, may be defined in three different ways.

1. In the simplest case misfit equates the rake difference :

$$m(i,j) = D\lambda_{ij} \tag{11.4}$$

2. When measurement error ranges, $\Delta\lambda_i^E$, are provided, they can be taken into account by setting the individual misfit as:
   - if $D\lambda_{ij} \leqslant \Delta\lambda_i^E$ then
   $$m(i,j) = 0 \tag{11.5}$$
   - if $D\lambda_{ij} > \Delta\lambda_i^E$ then
   $$m(i,j) = D\lambda_{ij} - \Delta\lambda_i^E \tag{11.6}$$

3. Finally for data where only slip sense is known, it may become :

- if $D\lambda_{ij} \leqslant 90°$ then
$$m(i,j) = 0 \tag{11.7}$$
- if $D\lambda_{ij} > 90°$ then
$$m(i,j) = 180 \tag{11.8}$$

For focal mechanisms, two misfits, one for each nodal plane, $m_a(i,j)$ and $m_b(i,j)$, can be computed as indicated above for the i$^{\text{th}}$ fault slip datum and j$^{\text{th}}$ stress datum. The individual misfit, $m(i,j)$, can be then computed in four ways:

1. by considering the 1$^{\text{st}}$ nodal plane only: $m(i,j) = m_a(i,j)$,
2. by considering the 2$^{\text{nd}}$ nodal plane only: $m(i,j) = m_b(i,j)$,
3. by taking the average: $m(i,j) = (m_a(i,j) + m_b(i,j))/2$, or
4. by taking the nodal plane with the lowest misfit: $m(i,j) = \min(m_a(i,j), m_b(i,j))$.

11.2.3 Global misfit

11.2.3.1 Global misfit for the full data set

When a full a set of N_{fs} fault slip data is taken into account the misfit, $M_F(j)$, for j$^{\text{th}}$ stress datum can be

- either the average of individual misfits
$$M_F(j) = \frac{1}{N_{fs}} \sum_{i=1}^{N_{fs}} m(i,j) \tag{11.9}$$
- or the maximum individual misfit
$$M_F(j) = \max\{m(i,j) : i = 1, \ldots, N_{fs}\} \tag{11.10}$$

11.2.3.2 Global misfit for a subset of the data

Requiring the stress solution to match only a subset of the data allows to identify and separate multiphase data (*Etchecopar et al.*, 1981; *Etchecopar*, 1984). The subset size is defined in the program as a percentage of the total number of data.

Calling P_{fs} the actual number of data to be matched
$$P_{fs} \leqslant N_{fs} \tag{11.11}$$
the data are first sorted to obtain $m(i,j)$ in ascending order:
$$m(1,j) \leqslant m(2,j) \leqslant \ldots \leqslant m(i,j) \leqslant \ldots \leqslant m(P_{fs},j) \leqslant \ldots \leqslant m(N_{fs},j) \tag{11.12}$$
The global misfit, $M_F(j)$, then retains the P_{fs} data with the lowest individual errors only and can be

- either the average of individual misfits

$$M_F(j) = \frac{1}{P_{fs}} \sum_{i=1}^{P_{fs}} m(i,j) \tag{11.13}$$

- or the maximum individual misfit

$$M_F(j) = \max\{m(i,j) : i = 1, \ldots, P_{fs}\} \tag{11.14}$$

11.2.4 Misfit function options set up

Options set up is accessible within the STTRANSEARCH subroutine through the command:

```
Modify inversion parameters ...........70
```

that leads to the SFSINV subroutine with the following menu:

```
@@@@@@@@@@@@@@@@@@@@@@@@@@@@@@@@@@@@@@@@@@@@@@@@@@@@@
@ subroutine sfsinv                   v5.7 2016-05-25
@====================================================
---------------------------------------------
INVERSION PARAMETERS
---------------------------------------------
switch name of current set up
   1    1st  fault plane
   1    rake difference
   1    Average on % best
---------------------------------------------
fault plane choice
1st  fault plane      .........101
---------------------------------------------
fault plane error
rake difference       .........201
slip sense            .........202
rake range difference .........203
---------------------------------------------
global error
Average on % best     .........301
Maximum on % best     .........302
-----------------------------------
% of data to explain ..........10    100.0
---------------------------------------------
EXIT ..........................99
@@@@@@@@@@@@@@@@@@@@@@@@@@@@@@@@@@@@@@@@@@@@@@@@@@@@@
```

11.3 Random search

The random search applies a Monte Carlo approach to seek a stress tensor best explains the slip directions. It mainly follows the method proposed by *Etchecopar et al.* (1981) and *Etchecopar* (1984) and implemented in their FAILLE program, and proceeds in 4 steps.

1. Reduced stress tensors parameters, $(\theta, \varphi, \psi, r_0)$, are generated by using a random suite X_k within [0,1] as follows
   - $\theta = X_k \cdot 360$
   - $\varphi = \arccos(X_{k+1})$
   - $\psi = X_{k+2} \cdot 180$
   - $r_0 = X_{k+3}$

   so that the orientations are uniformly distributed in space. To obtain a reasonable estimate, a minimum of $N_{st} = 1000$ tensors need to be generated; this the default value for N_{st}, but it can be modified.
2. For each tensor of index j, the misfits for each fault slip datum, $m(1, j), m(2, j), \ldots, m(N_{fs}, j)$, are computed.
3. For each tensor of index j, the global misfit, $M_F(j)$, is then computed.
4. The tensors are ranked by increasing value of $M_F(j)$ and only the N_{st0} first tensors are retained.

11.4 Optimisation

In this approach one of the 4 parameters $(\theta, \varphi, \psi, r_0)$ defining the reduced stress tensor is varied while the others are kept constant. The global error, $M_F(j)$, is computed as in the random search. The tensor with the lowest $M_F(j)$ value is retained. This can be used to refine solutions found by random search.

Table 11.1: Inversion parameters

Symbol	Definition & Comments
N_{fs}	Fault slip data set size
P_{fs}	Fault slip data subset size
i	Fault slip datum index $\quad i \in [1, N_{fs}]$
λ_i^A	Actual rake of i$^{\text{th}}$ datum
λ_i^M	Measured rake of i$^{\text{th}}$ datum: $\lambda_i^A = \lambda_i^M$ if the measurement is perfect
$\Delta\lambda_i^E$	Half error range on i$^{\text{th}}$ datum rake measurement $\Delta\lambda_i^E \in [0°, 180°] \quad \lambda_i^A \in \left[\lambda_i^M - \Delta\lambda_i^E, \lambda_i^M + \Delta\lambda_i^E\right]$
N_{st}	Number of stress tensor tested
N_{st0}	Number of stress tensor solutions retained
j	Stress tensor datum index $\quad j \in [1, N_{st}]$
λ_{ij}^P	Rake predicted by the j$^{\text{th}}$ stress datum on the i$^{\text{th}}$ fault datum (rake of predicted shear stress)
$\Delta\lambda_{ij}$	Difference between rake predicted by the j$^{\text{th}}$ stress datum and measured rake for the i$^{\text{th}}$ fault datum $\Delta\lambda_{ij} = \lambda_{ij}^P - \lambda_i^M \quad \Delta\lambda_{ij} \in [-180°, +180°]$
$D\lambda_{ij}$	Rake difference for the j$^{\text{th}}$ stress datum and i$^{\text{th}}$ fault datum $D\lambda_{ij} = \lvert\Delta\lambda_{ij}\rvert \quad D\lambda_{ij} \in [0°, 180°]$
$m(i,j)$	Misfit for i$^{\text{th}}$ fault datum and j$^{\text{th}}$ stress datum (individual misfit) $m(i,j) \in [0°, 180°]$
$m_a(i,j)$	Misfit for 1$^{\text{st}}$ nodal plane of i$^{\text{th}}$ fault datum and j$^{\text{th}}$ stress datum $m_a(i,j) \in [0°, 180°]$
$m_b(i,j)$	Misfit for 2$^{\text{nd}}$ nodal plane of i$^{\text{th}}$ fault datum and j$^{\text{th}}$ stress datum $m_b(i,j) \in [0°, 180°]$
$M_F(j)$	Misfit function for the fault slip data set and j$^{\text{th}}$ stress datum (global misfit) $M_F(j) \in [0°, 180°]$

Chapter 12

Analysing the relationship between stress and fault

12.1 Introduction

The required input are both N_{fs} fault slip and N_{st} stress data (parameters are summarized in Table 11.1).

12.2 Computations

In a first step, individual misfits, $m(i, j)$, for each fault slip datum of index i and stress datum of index j are computed, filling and array of size $N_{fs} \times N_{st}$.

In a second step step, the global misfit, $M_F(j)$, is computed for each stress tensor of index j according to the misfit function options, filling an array of size N_{st}.

This allows to produce multiple graphical representations of the relationship between stress and fault.

In what follows, we distinguish

- fault data indexes that are contiguous and correspond to the line number in the data file, i.e. the order in which the data are read, from
- fault data identification numbers that are read in the input file and do not need to be contiguous.

12.3 Graphical representations

Plots are grouped in three categories according to the number of data involved.

12.3.1 Global plots: N_{st} stress tensors and N_{fs} fault data

- Stereoplots of stress tensor axes and fault slip data
- Histograms of $M_F(j)$, r_{0j}
- Misfit function $M_F(j)$ versus stress tensor index j
- Checkerboard representation of $m(i, j)$

12.3.2 Plots for 1 stress tensor and N_{fs} fault data

With the stress datum of index j

- Histogram of misfits $m(i, j)$
- Misfits $m(i, j)$ versus fault slip data index i
- Value of $s_0 = (\sigma_1 - \sigma_3)/\sigma_1$ to activate each fault plane versus fault data index i
- Value of friction coefficient, μ, to activate each fault plane versus fault data index i
- Mohr's circles where fault slip data are displayed with their identification number

Explanations on the use of s_0 and μ can be found in the appendix of *Burg et al.* (2005).

12.3.3 Plots for one stress tensor and one fault slip datum

- Variation of shear stress, normal stress, and s_0 as a function of r_0

12.4 Tabulated output of misfits

Tabulated values of misfits, $m(i, j)$, and misfit function, $M_F(j)$, can be exported in an output file that can be imported in a spreadsheet.

12.5 Quality criteria for inversion results

Appendix A of *Heuberger et al.* (2010) proposes a way to use the results of this analysis to attribute quality criteria to inversion results in the case of polyphase data.

Part V

The program & computer environment

Chapter 13

References relevant to Fsa

13.1 How to refer to Fsa

If you publish results obtained with Fsa, it would be appreciated that you referred to:

- the software version and its location as:
  Celerier, B., YYYY, Fsa: Fault & Stress Analysis software, version XX.X,
  http://www.celerier.gm.univ-montp2.fr/software/dcmt/fsa/fsa.html.
  where XX.X and YYYY are the version and year of the software used that can be found in 2 places :
  - they are displayed in the console when the program starts, and
  - they are printed at the top of all plots.
- *Etchecopar et al.* (1981) who introduced the random search method, with the possibility to account for only part of the data in the case of multiphase data, that is implemented in Fsa;
- *Heuberger et al.* (2010) or *Burg et al.* (2005) who describe the methods implemented in Fsa and show examples of application;

13.2 Other relevant references

Below are a few additional relevant references ordered by subjects of interest.

- The random search method implemented in Fsa: *Etchecopar et al.* (1981); *Etchecopar* (1984).
- Original definition of $\phi = (\sigma_2 - \sigma_3)/(\sigma_1 - \sigma_3)$: *Angelier* (1975).

- Definition of $r_0 = (\sigma_1 - \sigma_2)/(\sigma_1 - \sigma_3)$ used in FSA: *Célérier* (1988, 1995, 2008); *Tajima and Célérier* (1989).
- Definition of $s_0 = (\sigma_1 - \sigma_3)/(\sigma_1)$ used in FSA: *Célérier* (1988, 2008); *Tajima and Célérier* (1989).
- Geometry of the optimal stress tensor for a single fault and slip datum: *Compton* (1966); *Etchecopar* (1984); *Célérier* (1988, 2008).
- Triangular representation of stress tensor axes: *Frohlich and Apperson* (1992); *Frohlich* (1992, 2001); Appendix B of *Célérier* (2008); *Célérier* (2010).
- The evaluation of friction conditions: Appendix A of *Burg et al.* (2005).
- The inversion of fault data with slip sense information only: *Lisle et al.* (2001); *Orife et al.* (2002). Note that, whereas the general idea originates from these papers, the inversion method implemented in FSA differs from that proposed in these references.
- Quality criteria for solutions in the case of polyphase data: Appendix A of *Heuberger et al.* (2010).
- Examples of application of FSA to fault and slip data: *Zeilinger et al.* (2000); *Célérier and Séranne* (2001); *Titus et al.* (2002); *Burg et al.* (2005); *Federico et al.* (2009, 2010, 2014, 2020); *Heuberger et al.* (2010); *Kounov et al.* (2010, 2011); *Dolati and Burg* (2013); *Mikolaichuk et al.* (2020); *Faucher et al.* (2021); *Cianfarra et al.* (2022).
- Examples of application of FSA to focal mechanism data: *Provost and Houston* (2001, 2003a,b); *Célérier* (2008); *Dolati and Burg* (2013); *Bauve et al.* (2014); *Plateaux et al.* (2014); *Rigo et al.* (2015).
- Examples of application of FSA to structural measurements in boreholes: *De Larouzière et al.* (1999); *Célérier et al.* (2002); *Louvel et al.* (2002)

Chapter 14

Fsa versions history

Fsa has been continuously evolving since an early prototype made in summer 1991. Originally developed on Sun workstations, it was ported to MacOS Classic, then to MacOS X. It has also been partially ported to Windows. Version history is summarized in Table 14.1.

Table 14.1: Fsa program versions

Version	Date	Comments
38.5	10 January 2025	Begin source conversion to f90.
38.4	14 September 2024	Adapt to upgraded libraries.
38.3	1 August 2022	Adapt to upgraded libraries.
38.2	28 February 2021	Adapt to upgraded libraries.
38.1	17 November 2020	Adapt to upgraded libraries.
38.0	19 October 2020	Adapt to upgraded libraries.
37.6	24 September 2020	Revise output file file name and title.
37.5	9 July 2020	Revise file name length and defaults.
37.4	8 May 2020	Add labels to s_0 lines in Mohr's representation.
37.3	19 November 2019	Clarify nodal plane choice in menus.
37.2	27 July 2019	Improve data description menus.
37.1	8 April 2019	Upgrade fault and stress data outputs and fault data display.
37.0	30 May 2018	Terminate upgrade of input of fault data as dip direction, dip, trend, plunge to output of a clearer and more complete error listing.
36.9	23 May 2018	Begin upgrade of input of fault data as dip direction, dip, trend, plunge to output of a clearer and more complete error listing.
36.8	18 January 2018	Terminate upgrade of math libraries.
36.7	25 July 2017	Upgrade plot landscape/portrait set up.

Table 14.1: (continued)

Version	Date	Comments
36.6	14 March 2017	Begin upgrade of math libraries.
36.5	29 November 2016	Modify axis range in tensor optimisation plots.
36.4	17 November 2016	Output of azimuth and plunge of slip vectors for FPS+3D coord and CPS+3D coord. Fix frame of slip trend rose diagram.
36.3	20 October 2016	Changes in menus and dialogs.
36.2	10 October 2016	Data format names and labels reorganized and documented.
36.1	27 May 2016	More use of color for fs in analysis.
36.0	25 May 2016	Use more efficient stereos for fs in analysis. Step 2: with color.
35.5	19 May 2016	Use more efficient stereos for fs in analysis. Step 1: without color.
35.4	15 July 2015	Dip, dip direction, plunge, trend input for fs.
35.3	27 February 2015	Fault plane only data output.
35.2	5 July 2013	Control on id in Breddin's plots.
35.1	2 June 2013	Add slip trend and plunge histograms.
35.0	12 Avril 2013	Fault and slip display upgrade: menu change, more plot options.
34.5	9 Avril 2013	Adapt axes to larger number of data (>100 000); wider console.
34.4	8 March 2013	More consistent mapping symbols.
34.3	26 February 2013	Adapt outputs to larger number of data (>100 000).
34.2	17 November 2012	Stereographic projection upgrade.
34.1	26 April 2012	Run time information upgrade.
34.0	11 November 2011	More use of improved stereographic projection.
33.9	10 November 2011	More control on axes set up.
33.8	1 March 2011	More mapping contours formats.
33.7	24 January 2011	Upgrade of analysis tabulated output.
33.6	14 May 2010	Quartz library interface update.
33.5	27 April 2010	Add beach ball plot of fault plane solutions.
33.4	21 April 2010	Add HASH (*Hauksson et al.*, 2012; *Yang et al.*, 2012) input for fault plane solutions.
33.3	29 January 2010	X-Y grids for maps.
33.2	30 November 2009	Direct computation of P,B,T from nodal planes.
33.1	24 November 2009	Mapping faults and slip vectors.
33.0	12 October 2009	Upgrade triangular diagrams: more projections, improved axes.
32.4	06 September 2009	Improve histograms axes.
32.3	04 September 2009	Upgrade histogram library.

Table 14.1: (continued)

Version	Date	Comments
32.2	18 May 2009	Optional color coding and graphic output (345/346) for analysis, map clipping, alternate axis symbol for stereographic projections standardized.
32.1	22 April 2009	Add computation of optimal conjugate planes from stress tensor orientation and input of focal mechanisms given by P and T axes only.
32.0	1 April 2009	Shorten inversion calculations.
31.1	19 March 2009	Plot librairies upgrade.
31.0	27 February 2009	Conjugate planes with slip data type added.
30.5	17 December 2008	Slip trend, plunge input and verification that slip is within the fault plane.
30.4	16 December 2008	Slip trend, plunge input.
30.3	01 December 2008	Slip trend, plunge output.
30.2	07 May 2008	P, B, T input.
30.1	10 April 2008	Inversion parameters menu upgrade.
30.0	28 March 2008	More coastline files for mapping.
29.9	18 February 2008	Axes upgrade.
29.8	09 January 2008	Input file error management upgrade. Checkerbox plot legend. AzShmax normalisation.
29.7	26 November 2007	Histogram library upgrade.
29.6	26 September 2007	Reorganize static libraries.
29.5	01 September 2007	Fix axis label in single fault analysis.
29.4	20 August 2007	Modify stress tensor set up and input.
29.3	05 August 2007	Modify fault and slip set up and input.
29.2	12 June 2007	Random fault and slip generation.
29.1	12 March 2007	Superposed histograms: stable solution.
29.0	07 January 2007	Axes upgrade.
28.8	05 October 2006	Add tabulated Etchecopar format to fault slip and bedding input.
28.7	25 July 2006	Superposed histograms: temporary solution.
28.6	14 June 2006	Plunge compensated histograms.
28.5	12 May 2006	Extra Mohr space friction line options.
28.4	18 April 2006	Extra stress directions mapping options.
28.3	01 December 2005	MacOSX Quartz version. Axis library upgrade.
28.2	01 September 2005	Comprehensive analysis spreadsheet friendly output file.
28.1	22 August 2005	Basic analysis output file.
28.0	07 March 2005	Stress projection for mapping.
27.6	27 January 2005	Stereo upgrade for large number of data.
27.5	09 June 2004	Rose diagrams.
27.4	02 June 2004	Enhance axis and analysis.
27.3	17 February 2004	Internal reorganisation.

Table 14.1: (continued)

Version	Date	Comments
27.2	10 November 2003	Single fault - single stress tensor analysis. More flexible axis library.
27.1	04 November 2003	Internal reorganisation.
27.0	31 October 2003	Optimal stress.
26.8	08 October 2003	Single plane FPS input, stereos upgrade, rake plots.
26.7	04 September 2003	Axis library upgrade.
26.6	07 July 2003	Separate stereos for explained and unexplained data. Friction lines for s_0 = 0.68,0.8,1.0.
26.5	20 March 2003	Add error function = max of errors.
26.4	02 December 2002	Add inversion with rake range.
26.3	17 November 2002	Optimization of solutions.
26.2	05 November 2002	More analysis options.
26.1	26 October 2002	Projection library upgrade.
26.0	24 October 2002	Triangular diagram upgrade. Stress id.
25.2	11 October 2002	Add tectonic regime plot.
25.1	03 September 2002	Projection library upgrade.
25.0	12 July 2002	Add stress tensor location and stress axis horizontal projection mapping.
24.4	20 June 2002	Stress tensor parameters histograms. Normalized angles.
24.3	11 June 2002	More fault plane input format (ef,em).
24.2	13 December 2001	More color options.
24.1	28 November 2001	Improved histogram axis.
24.0	18 August 2001	Add slip sense only inversion, as in *Lisle et al.* (2001).
23.2	15 June 2001	Add stress tensor display: stereos and *Frohlich*'s (1992; 2001) triangular diagrams.
22.0	06 June 2001	Fault plane solution (FPS) input, display, inversion (both or best), and analysis. Maximum set to 500 fps x 300 tensors. Calculations take more advantage of the reduced stress tensor matrix structure and are therefore 170% faster.
21.2	31 October 2000	Add command files and fault plane (without slip) input & display. Geoframe format input for borehole fracture analysis.
20.7	04 September 2000	Stress tensor input and output. Note that the stress file header is now only 2 lines long, as in FSA18.8, but as opposed to FSA18.7 and older where it is 3 lines long.
20.5	02 February 2000	Stress & fault analysis.
20.4	05 January 2000	Random tensor search.
20.3	06 November 1999	New stress tensor structure.
20.2	30 May 1999	Update data type.

Table 14.1: (continued)

Version	Date	Comments
20.1	27 May 1999	Update histograms.
20.0	14 May 1999	New histograms library.
19.2	31 January 1999	Rotates fault data around an horizontal axis.
19.1	29 December 1998	Reads + displays fault data.
19.0	13 May 1998	Begin development of a new thread based on a new data structure. New fault data structure implemented (no stress tensor yet).
18.9	22 May 2001	Calculations take more advantage of the reduced stress tensor matrix structure and are therefore 170% faster. After this version, all further development is done in the new thread starting at FSA19.0 because FSA22.0 already has more functionalities than FSA18.9 in particular for focal mechanisms. However, this version remains available because of a few of its functions that are not yet included in the newer versions.
18.8	04 September 2000	Stress tensor file format header changed from 3 lines to 2 lines. Note that old stress tensor files generated by FSA18.7 can still be read by changing the number of header lines to skip from 2 to 3.
18.7	06 March 2000	Introduces command files to automatize processing. Upgrade synthetic faults generation.
18.6	29 November 1999	Macintosh version: portrait set up option for -qdraw allows to keep the window from covering all the screen.
18.6	8 November 1999	Plot up to 1000 data. Revised PostScript: all 3 options (Compressed, NeWS and Illustrator v.2) should open with Adobe Illustrator. Best choices are NeWS (Default) or Compressed (smaller files but same quality as NeWS).
18.6	13 September 1999	Good news: FSA18.6 can read up to 1000 fault data instead of 300 in previous versions. Bad news: for Macintosh version, FSA18.6 needs around 9.5MB of RAM instead of 3.5MB in previous versions.
18.5	11 June 1999	ASCII output of analysis.
18.4	20 April 1999	More tensor output formats.

Table 14.1: (continued)

Version	Date	Comments
18.3	15 April 1999	Changes in graphical display. More tensor output formats. The Macintosh version is compiled with a higher degree of backgrounding. It is expected to be 25% slower but it let you work with other applications while it is running. This may also avoid the problem caused when Eudora tries to check mail while FSA is running, that could result in system crashes in previous versions.
18.2	10 December 1997	Add synthetic rakes.
18.1	3 November 1997	Upgrade Mohr's frame.
18.0	30 October 1997	Add tensor search and optimization on a % of the data.
17.0	29 October 1997	Add fault data display and simplify PostScript file management. It is now easier to close and reopen a new PostScript file to avoid overlays.
16.3	19 September 1997	Continue improving plot file management.
16.2	15 September 1997	Improve plot file management.
16.1	19 June 1997	Add run time information.
16.0	14 May 1997	Add Mohr circle analysis. New PowerPC optimized version for Macintosh.
15.2	30April 1997	Tensor labels.
15.1	10 February 1997	Add synthetics and tabulated Etchecopar format.
15.0	7 May 1996	Change stress tensor data structure. The program takes its current name: FSA.
14.3[1]	19 April 1996	Add output of stress data
14.2[1]	18 April 1996	Add input of stress data
14.1[1]	10 April 1996	Add output of fault and slip data
14.0[1]	4 March 1996	Analysis decoupled from random search
13.0[1]	25 December 1995	Add single fault and tensor analysis.
12.0[1]	12 October 1995	Add optimal stress.
11.0[1]	4 October 1995	Internal upgrade.
10.0[1]	3 October 1995	Upgrade calculations and analysis.
9.0[1]	29 July 1995	Upgrade graphics.
8.0[1]	21 July 1995	Upgrade calculations and graphics.
7.0[1]	10 August 1993	SunOS with GKS port.
6.0[1]	22 July 1992	MacOS Classic port.
6.0[1]	6 August 1991	Improve and test calculations. Succesfully tested against Etchecopar's FAILLE.
5.0[1]	31 July 1991	Improve and test calculations. Extend graphics.
4.0[1]	26 July 1991	Improve and test calculations. Extend graphics.
3.0[1]	16 July 1991	Improve and test calculations. Extend graphics.

[1]The program was named FSI from versions 1.0 to 15.0

Table 14.1: (continued)

Version	Date	Comments
2.0[1]	13 July 1991	Add graphics using Sun CGI.
1.0[1]	9 July 1991	First prototype, FSI, on SunOS. Input of fault and slip data, random tensor search, selection and output of the best stress tensor. No graphics.

Bibliography

Aki, K., and P. G. Richards (1980), *Quantitative seismology; Theory and methods*, vol. I, 557 pp., W.H. Freeman and Company, San Francisco.

Aki, K., and P. G. Richards (2002), *Quantitative seismology - Second Edition*, 700 pp., University Science Books, Sausalito, California.

Anderson, E. M. (1905), The dynamics of faulting, *Transactions of the Edinburgh Geological Society*, *8*, 387–402.

Anderson, E. M. (1951), *The dynamics of faulting and dyke formation with applications to Britain*, 2nd edition ed., 206 pp., Oliver and Boyd, Edinburgh.

Anderson, E. M. (2012), Facsimile reproduction of 'The dynamics of faulting' by E. M. Anderson, *Geological Society, London, Special Publications*, *367*, 231–246, doi:10.1144/SP367.16.

Angelier, J. (1975), Sur l'analyse de mesures recueillies dans des sites faillés: l'utilité d'une confrontation entre les méthodes dynamiques et cinématiques, *C. R. Acad. Sci., Série D*, *281*, 1805–1808.

Armijo, R., E. Carey, and A. Cisternas (1982), The inverse problem in microtectonics and the separation of tectonic phases, *Tectonophysics*, *82*(1), 145–160, doi:10.1016/0040-1951(82)90092-0.

Arthaud, F. (1969), Méthode de détermination graphique des directions de raccourcissement, d'allongement et intermédiaire d'une population de failles, *Bulletin de la Societé Géologique de France*, *7*(XI), 729–737, doi:10.2113/gssgfbull.S7-XI.5.729.

Bauve, V., R. Plateaux, Y. Rolland, G. Sanchez, N. Bethoux, B. Delouis, and R. Darnault (2014), Long-lasting transcurrent tectonics in SW Alps evidenced by Neogene to present-day stress fields, *Tectonophysics*, *621*, 85 – 100, doi:10.1016/j.tecto.2014.02.006.

Bucher, W. H. (1920), The mechanical interpretation of joints. Part I, *The Journal of Geology*, *28*(8), 707–730, doi:10.1086/622744.

Bucher, W. H. (1921), The mechanical interpretation of joints. Part II, *The Journal of Geology*, *29*(1), 1–28, doi:10.1086/622751.

Burg, J.-P., B. Célérier, N. M. Chaudhry, M. Ghazanfar, F. Gnehm, and M. Schnellmann

(2005), Fault analysis and paleostress evolution in large strain regions: methodological and geological discussion of the southeastern Himalayan fold-and-thrust belt in Pakistan, *Journal of Asian Earth Sciences*, *24*(4), 445 – 467, doi:10.1016/j.jseaes.2003.12.008.

Célérier, B. (1988), How much does slip on reactivated fault plane constrain the stress tensor ?, *Tectonics*, *7*(6), 1257–1278, doi:10.1029/TC007i006p01257.

Célérier, B. (1995), Tectonic regime and slip orientation of reactivated faults, *Geophysical Journal International*, *121*(1), 143–191, doi:10.1111/j.1365-246X.1995.tb03517.x\&10.1111/j.1365-246X.1995.tb07021.x.

Célérier, B. (2008), Seeking Anderson's faulting in seismicity: a centennial celebration, *Review of Geophysics*, *46*(4), RG4001, 1–34, doi:10.1029/2007RG000240.

Célérier, B. (2010), Remarks on the relationship between the tectonic regime, the rake of the slip vectors, the dip of the nodal planes, and the plunges of the P, B, and T axes of earthquake focal mechanisms, *Tectonophysics*, *482*(1-4), 42–49, doi:10.1016/j.tecto.2009.03.006.

Célérier, B., and M. Séranne (2001), Breddin's graph for tectonic regimes, *Journal of Structural Geology*, *23*(5), 789–801, doi:10.1016/S0191-8141(00)00140-1\&10.1016/S0191-8141(01)00058-X.

Célérier, B., V. Louvel, B. Le Gall, V. Gardien, and P. Huchon (2002), Presentation and structural analysis of FMS electrical images in the northern margin of the Woodlark Basin, in *Proceedings of the Ocean Drilling Program, Scientific Results*, vol. 180, edited by B. Taylor, P. Huchon, and A. Klaus, pp. 1–159, Ocean Drilling Program, College Station, Texas, doi:10.2973/odp.proc.sr.180.177.2002.

Célérier, B., A. Etchecopar, F. Bergerat, P. Vergely, F. Arthaud, and P. Laurent (2012), Inferring stress from faulting: from early concepts to inverse methods, *Tectonophysics*, *581*, 206–219, doi:10.1016/j.tecto.2012.02.009.

Cianfarra, P., M. Locatelli, G. Capponi, L. Crispini, C. Rossi, F. Salvini, and L. Federico (2022), Multiple reactivations of the Rennick graben fault system (Northern Victoria Land, Antarctica): New evidence from paleostress analysis, *Tectonics*, *41*(6), 1–25, doi:10.1029/2021TC007124.

Compton, R. R. (1966), Analyses of Pliocene-Pleistocene deformation and stresses in northern Santa Lucia Range, California, *Geological Society of America Bulletin*, *77*(12), 1361–1379, doi:10.1130/0016-7606(1966)77[1361:AOPDAS]2.0.CO;2.

De Larouzière, F. D., P. A. Pézard, M. C. Comas, B. Célérier, and C. Vergniault (1999), Structure and tectonic stresses in metamorphic basement, Site 976, Alboran sea, in *Proceedings of the Ocean Drilling Program, Scientific Results*, vol. 161, edited by R. Zahn, M. C. Comas, and A. Klaus, pp. 319–329, Ocean Drilling Program, College Station, Texas, doi:10.2973/odp.proc.sr.161.212.1999.

Dolati, A., and J. P. Burg (2013), Preliminary fault analysis and paleostress evolution in the Makran fold-and-thrust belt in Iran, in *Lithosphere Dynamics and Sedimentary Basins: The Arabian Plate and Analogues*, edited by K. Al Hosani, F. Roure, R. Ellison, and S. Lokier, pp. 261–277, Springer Berlin Heidelberg, doi:10.1007/978-3-642-30609-9_13.

Etchecopar, A. (1984), Étude des états de contrainte en tectonique cassante et simulations de déformations plastiques (approche mathématique). Thèse d'État, Ph.D. thesis, Université des Sciences et Techniques du Languedoc.

Etchecopar, A., G. Vasseur, and M. Daignieres (1981), An inverse problem in microtectonics for the determination of stress tensors from fault striation analysis, *Journal of Structural Geology*, *3*(1), 51–65, doi:10.1016/0191-8141(81)90056-0.

Euler, L. (1767), Du mouvement d'un corps solide quelconque lorsqu'il tourne autour d'un axe mobile, *Mémoires de l'Académie des sciences de Berlin*, *[16], (1760)*, 176–227.

Faucher, A., F. Gueydan, M. Jolivet, M. Alsaif, and B. Célérier (2021), Dextral strike-slip and normal faulting during Mid-Miocene back-arc extension and westward Anatolia extrusion in Central Greece, *Tectonics*, *40*(6, e2020TC006615), doi:10.1029/2020TC006615.

Federico, L., C. Spagnolo, L. Crispini, and G. Capponi (2009), Fault-slip analysis in the metaophiolites of the Voltri massif: constraints for the tectonic evolution at the Alps/Apennine boundary, *Geological Journal*, *44*(2), 225–240, doi:10.1002/gj.1139.

Federico, L., L. Crispini, and G. Capponi (2010), Fault–slip analysis and transpressional tectonics: A study of Paleozoic structures in northern Victoria Land, Antarctica, *Journal of Structural Geology*, *32*(5), 667 – 684, doi:10.1016/j.jsg.2010.04.001.

Federico, L., L. Crispini, A. Vigo, and G. Capponi (2014), Unravelling polyphase brittle tectonics through multi-software fault-slip analysis: The case of the Voltri Unit, Western Alps (Italy), *Journal of Structural Geology*, *68*, 175 – 193, doi:10.1016/j.jsg.2014.09.011.

Federico, L., M. Maino, G. Capponi, and L. Crispini (2020), Paleo-depth of fossil faults estimated from paleostress state: applications from the Alps and the Apennines (Italy), *Journal of Structural Geology*, *140*, 1–16, doi:10.1016/j.jsg.2020.104152.

Friedman, M. (1964), Petrofabric techniques for the determination of principal stress directions in rocks, in *State of stress in the earth's crust, proceedings of the international conference June 13-14, 1963, Santa Monica, California*, edited by W. R. Judd, pp. 451–552, American Elsevier Publishing Co., New York.

Frohlich, C. (1992), Triangle diagrams: ternary graphs to display similarity and diversity of earthquake focal mechanisms, *Physics of the Earth and Planetary Interiors*, *75*(1), 193–198, doi:10.1016/0031-9201(92)90130-N.

Frohlich, C. (2001), Display and quantitative assessment of distributions of earthquake

focal mechanisms, *Geophysical Journal International*, *144*(2), 300–308, doi:10.1046/j.1365-246x.2001.00341.x.

Frohlich, C., and K. D. Apperson (1992), Earthquake focal mechanisms, moment tensors, and the consistency of seismic activity near plate boundaries, *Tectonics*, *11*(2), 279–296, doi:10.1029/91TC02888.

Guiraud, M., O. Laborde, and H. Philip (1989), Characterization of various types of deformation and their corresponding deviatoric stress tensors using microfault analysis, *Tectonophysics*, *170*(3), 289–316, doi:10.1016/0040-1951(89)90277-1.

Harland, W. B., and M. B. Bayly (1958), Tectonic regimes, *Geological Magazine*, *95*(2), 89–104, doi:10.1017/S0016756800062671.

Hauksson, E., W. Yang, and P. M. Shearer (2012), Waveform relocated earthquake catalog for southern California (1981 to june 2011), *Bulletin of the Seismological Society of America*, *102*(5), 2239–2244, doi:10.1785/0120120010.

Heuberger, S., B. Célérier, J. P. Burg, N. M. Chaudhry, H. Dawood, and S. Hussain (2010), Paleostress regimes from brittle structures of the Karakoram-Kohistan suture zone and surrounding areas of NW Pakistan, *Journal of Asian Earth Sciences*, *38*(6), 307–335, doi:10.1016/j.jseaes.2010.01.004.

Hoskins, L. M. (1896), Flow and fracture of rocks as related to structure, in *Sixteenth annual report of the United States Geological Survey to the Secretary of the Interior, 1894-1895: Part 1*, edited by D. Walcott, pp. 845–874, USGS.

Huang, Q., and J. Angelier (1987), Les systèmes de failles conjuguées: une méthode d'identification, de séparation et de calcul des axes de contrainte, *C. R. Acad. Sci., Série II*, *304*(9), 465–468.

Huang, Q., and J. Angelier (1989), Inversion of field data in fault tectonics to obtain the regional stress - II. Using conjugate fault sets within heterogeneous families for computing palaeostress axes, *Geophysical Journal International*, *96*(1), 139–149, doi:10.1111/j.1365-246X.1989.tb05256.x.

Hubbert, K. (1951), Mechanical basis for certain familiar geologic structures, *Bulletin of the Geological Society of America*, *62*(4), 355–372, doi:10.1130/0016-7606(1951)62[355:MBFCFG]2.0.CO;2.

Hubbert, K. (1972), Introduction - Phenomena of structural geology, in *Structural geology*, edited by K. Hubbert, pp. 1–19, Hafner publishing co.

Kaverina, A. N., A. V. Lander, and A. G. Prozorov (1996), Global creepex distribution and its relation to earthquake-source geometry and tectonic origin, *Geophysical Journal International*, *125*(1), 249–265, doi:10.1111/j.1365-246X.1996.tb06549.x.

Kounov, A., D. Seward, J.-P. Burg, D. Bernoulli, Z. Ivanov, and R. Handler (2010), Geochronological and structural constraints on the cretaceous thermotectonic evolution

of the kraishte zone, western bulgaria, *Tectonics*, *29*(2, TC2002), 1–19, doi:10.1029/2009TC002509.

Kounov, A., J.-P. Burg, D. Bernoulli, D. Seward, Z. Ivanov, D. Dimov, and I. Gerdjikov (2011), Paleostress analysis of Cenozoic faulting in the Kraishte area, SW Bulgaria, *Journal of Structural Geology*, *33*(5), 859 – 874, doi:10.1016/j.jsg.2011.03.006.

Lisle, R., T. Orife, and L. Arlegui (2001), A stress inversion method requiring only fault slip sense, *Journal of Geophysical Research: Solid Earth*, *106*(B2), 2281–2289, doi:10.1029/2000JB900353.

Louvel, V., B. Le Gall, B. Célérier, V. Gardien, and P. Huchon (2002), Structural analysis of the footwall fault block of the Moresby detachment (Woodlark rift basin) from borehole images, in *Proceedings of the Ocean Drilling Program, Scientific Results*, vol. 180, edited by B. Taylor, P. Huchon, and A. Klaus, pp. 1–43, Ocean Drilling Program, College Station, Texas, doi:10.2973/odp.proc.sr.180.165.2002.

McKenzie, D. P. (1969), The relation between fault plane solutions for earthquakes and the directions of the principal stresses, *Bulletin of the Seismological Society of America*, *59*(2), 591–601, doi:10.1785/BSSA0590020591.

Mikolaichuk, A. V., Z. A. Kalmetyeva, J. P. Burg, D. Fossati, and D. V. Gordeev (2020), Seismotectonics of the inner Tienshan: Suusamyr basin and adjacent areas, *Geodynamics & Tectonophysics*, *11*(1), 39–52, doi:10.5800/GT-2020-11-1-0461.

Orife, T., L. Arlegui, and R. J. Lisle (2002), Dipslip: a quickbasic stress inversion program for analysing sets of faults without slip lineations, *Computers & Geosciences*, *28*(6), 775 – 781, doi:DOI:10.1016/S0098-3004(01)00099-1.

Philip, H. (1987), Plio-Quaternary evolution of the stress field in Mediterranean zones of subduction and collision, *Annales Geophysicae*, *5B*, 301–320.

Plateaux, R., N. Béthoux, F. Bergerat, and B. Mercier de Lépinay (2014), Volcano-tectonic interactions revealed by inversion of focal mechanisms: stress field insight around and beneath the Vatnajökull ice cap in Iceland, *Frontiers in Earth Science*, *2*, 1–21, doi:10.3389/feart.2014.00009.

Provost, A.-S., and H. Houston (2001), Orientation of the stress field surrounding the creeping section of the San Andreas fault: Evidence for a narrow mechanically weak fault zone, *Journal of Geophysical Research: Solid Earth*, *106*(B6), 11,373–11,386, doi:10.1029/2001JB900007.

Provost, A.-S., and H. Houston (2003a), Stress orientations in northern and central California: Evidence for the evolution of frictional strength along the San Andreas plate boundary system, *Journal of Geophysical Research: Solid Earth*, *108*(B3), doi:10.1029/2001JB001123.

Provost, A.-S., and H. Houston (2003b), Investigation of temporal variations in stress

orientations before and after four major earthquakes in California, *Physics of the Earth and Planetary Interiors*, *139*(3), 255 – 267, doi:10.1016/j.pepi.2003.09.007.

Reasenberg, P. A., and D. Oppenheimer (1985), *FPFIT, FPPLOT, and FPPAGE: Fortran computer programs for calculating and displaying earthquake fault-plane solutions*, *Open-File Report*, vol. 85-739, 109 pp., U.S. Geological Survey.

Rigo, A., P. Vernant, K. L. Feigl, X. Goula, G. Khazaradze, J. Talaya, L. Morel, J. Nicolas, S. Baize, J. Chéry, and M. Sylvander (2015), Present-day deformation of the Pyrenees revealed by GPS surveying and earthquake focal mechanisms until 2011, *Geophysical Journal International*, *201*(2), 947–964, doi:10.1093/gji/ggv052.

Schmidt, W. (1925), XXIII. Gefügestatistik, *Tschermaks mineralogische und petrographische Mitteilungen*, *38*(1), 392–423, doi:10.1007/BF02993943.

Tajima, F., and B. Célérier (1989), Possible focal mechanism change during reactivation of a previously ruptured subduction zone, *Geophysical Journal International*, *98*(2), 301–316, doi:10.1111/j.1365-246X.1989.tb03354.x.

Titus, S., H. Fossen, R. Pedersen, J. Vigneresse, and B. Tikoff (2002), Pull-apart formation and strike-slip partitioning in an obliquely divergent setting, Leka ophiolite, Norway, *Tectonophysics*, *354*(1), 101 – 119, doi:10.1016/S0040-1951(02)00293-7.

Van Hise, C. R. (1896), Principles of North American Pre-Cambrian geology, in *Sixteenth annual report of the United States Geological Survey to the Secretary of the Interior, 1894-1895. Part 1*, edited by D. Walcott, pp. 571–843, USGS.

Wulff, G. (1902), Untersuchungen im Gebiete der optischen Eigenschaften isomorpher Krystalle, *Zeitschrift für Kristallographie und Mineralogie*, *36*, 1–28.

Yang, W., E. Hauksson, and P. M. Shearer (2012), Computing a large refined catalog of focal mechanisms for southern California (1981–2010): Temporal stability of the style of faulting, *Bulletin of the Seismological Society of America*, *102*(3), 1179–1194, doi:10.1785/0120110311.

Zeilinger, G., J. P. Burg, N. Chaudhry, H. Dawood, and S. Hussain (2000), Fault systems and Paleo-stress tensors in the Indus suture zone (NW Pakistan), *Journal of Asian Earth Sciences*, *18*(5), 547 – 559, doi:10.1016/S1367-9120(99)00084-X.